

## Highlights

### **Hierarchical $p$ -Adic Framework for Gene Regulatory Networks: Theory and Stability Analysis**

J. R. Pérez-Buendía, Víctor Nopal-Coello

- $p$ -Adic fractal (nested-ball) structure for multi-scale stability in GRNs.
- Stability measure  $\mu$  and optimal gene ordering; minimization over all  $N!$  orderings identifies master regulators.
- Ball-level classification of fixed points (contracting, expanding, isometric).
- *A. thaliana* ( $N = 13$ ): minimizing order places UFO, EMF1, LFY, TFL1 first; IEAA vs. IEEE patterns.
- Minimization recovers a partial order on genes—not presupposed—that agrees with the known developmental hierarchy.

# Hierarchical $p$ -Adic Framework for Gene Regulatory Networks: Theory and Stability Analysis

J. R. Pérez-Buendía<sup>a,\*</sup>, Víctor Nopal-Coello<sup>b</sup>

<sup>a</sup>SECIHTI-CIMAT, Unidad Mérida, Mérida, Yucatán, México,

<sup>b</sup>Universidad Autónoma del Estado de Hidalgo, Pachuca, Hidalgo, México,

---

## ARTICLE INFO

### Keywords:

2020 MSC: 11S82

37P20

92B05

$p$ -adic dynamics

fractal hierarchy

gene regulatory networks

ultrametric

hierarchical stability

master regulators

## Abstract

Gene regulatory networks exhibit hierarchical organization across scales; capturing this structure mathematically requires a metric that distinguishes regulatory influence at each level. We show that the ultrametric of the  $p$ -adic integers  $\mathbb{Z}_p$ —whose self-similar nested-ball structure is a natural fractal encoding of multi-scale organization—provides such a framework. Embedding the  $N$ -gene state space into  $\mathbb{Z}_p$  and working over the complete, algebraically closed field  $C_p$ , we prove the existence of rational functions that interpret the discrete dynamics and construct hierarchical approximations at each resolution level. These constructions yield a stability measure  $\mu$ —aggregating how the dynamics contracts or expands across resolution levels—and a ball-level classification of fixed points—contracting, expanding, or isometric—extending the attracting/repelling/indifferent trichotomy of non-Archimedean dynamics from points to balls. A key result is that  $\mu$  and the classification, although their definition and dynamical meaning require the analytical tools of  $C_p$ , are fully determined by the discrete data. Minimizing  $\mu$  over all  $N!$  gene orderings defines an optimal regulatory hierarchy; for the *Arabidopsis thaliana* floral development network ( $N=13$ ,  $p=2$ ), a  $\mu$ -minimizing ordering places known master regulators—UFO, EMF1, LFY, TFL1—in the leading positions and recovers the accepted developmental hierarchy without biological input beyond the transition map.

---

## 1. Introduction

Gene regulatory networks (GRNs) underlie how biological systems respond to stimuli, orchestrating cell differentiation, organ development, and adaptation; perturbations in regulatory genes can propagate and alter phenotypic outcomes [1, 4]. Identifying the most influential components and how perturbations affect global behavior remains a central challenge. Open questions include: which genes are critical for stability, how noise affects developmental trajectories, and which mathematical structures capture the layered, hierarchical nature of genetic regulation.

The present work develops a framework based on non-Archimedean dynamics for the long-term behavior of gene expression from a hierarchical viewpoint. The  $p$ -adic field carries a natural *fractal structure*: nested balls at scales  $1/p^n$ , each ball at scale  $n$  refining into  $p$  sub-balls at  $n + 1$ , with the same pattern at every scale. This structure yields rigorous results on stability and on the role of master regulators, via a stability measure  $\mu$  and a ball-level classification of fixed points. The article is centred on the *mathematics*; a concrete application to a floral development network illustrates the theory. Numerical evaluation of  $\mu$  and of the orderings is used where it supports or illustrates the mathematical development.

Traditional models—differential equations, Boolean networks, and probabilistic frameworks—have provided valuable insights into GRN dynamics [22, 35]; a recent meta-analysis confirms canalization, redundancy, and stability as design principles of regulatory logic [24]. Algebraic methods have supported network reconstruction, while probabilistic techniques capture uncertainty and variability. However, many such models rely on assumptions of linearity or uniform interactions, limiting their ability to reflect the complex, nonlinear, and hierarchical interactions inherent to biological regulation. Classical discrete dynamics on finite spaces treat configurations uniformly with respect to regulatory proximity, and hierarchical dependencies and stability patterns remain implicit in the transition graph.

We model the GRN as a discrete dynamical system. The configuration space  $C$  consists of all possible states of the  $N$  genes (each gene in  $\{0, \dots, p - 1\}$ , so  $|C| = p^N$ ), and the dynamics is given by a map  $f : C \rightarrow C$  (e.g. synchronous update of Boolean or logical rules). The gene ordering induces an encoding  $\iota$  of configurations as integers in base  $p$ ;

---

\*Corresponding author

✉ rogelio.perez@cimat.mx (J. R. Pérez-Buendía); victor.nopal@uaeh.edu.mx (V. Nopal-Coello)

ORCID(s): 0000-0002-7739-4779 (J. R. Pérez-Buendía); 0000-0003-2608-3636 (V. Nopal-Coello)

the pair  $(f, \iota)$  fixes both the transition rule and the hierarchical view we take. Main notation is collected in Section 1 (Table 1). We embed this structure into an ultrametric space (the  $p$ -adic numbers), where distance and nested balls reflect multi-scale organization (Section 2). The *existence* of a global rational function  $\phi$  that interprets  $f$  (Section 3) is essential: it is what allows us to use the tools of non-Archimedean dynamics and  $p$ -adic fixed-point theory (e.g. [5]). At the same time, the stability measure  $\mu$  and the ball-level classification of fixed points turn out to be computable from  $(f, \iota)$  alone (Theorem 5.5), so practical evaluation does not require constructing  $\phi$  explicitly; the theoretical framework in  $\mathbb{C}_p$ , however, is what gives these quantities their dynamical meaning and justifies the classification (Section 5).

At each resolution  $n$ , the partition of  $\mathbb{Z}_p$  into balls  $B_{1/p^n}(m)$  may be viewed as a finite family of observable states: two configurations are indistinguishable at level  $n$  precisely when they lie in the same ball. In this sense, the  $p$ -adic embedding does not merely encode the finite dynamics; it equips it with a hierarchy of observational scales. The rational interpreter  $\phi$  then induces the evolution of these observables across resolutions, while the stability measure  $\mu$  quantifies how often the dynamics expands rather than concentrates observable uncertainty.

Master regulators are familiar in development (e.g. LFY in floral identity [6, 37], cdc-25.1 in the cell cycle [3, 9]). The measure  $\mu$  and the notion of optimal ordering give a precise way to quantify their impact. Related  $p$ -adic work in biology includes overviews and applications [17], non-Archimedean replicator dynamics [39], reaction-diffusion models [19], non-Archimedean morphogenesis [40], and  $p$ -adic neural networks [38]. This work applies  $p$ -adic methods to hierarchical stability in GRNs via rational approximations. Boolean models for *A. thaliana* [18, 27] and related work on epigenetic landscapes—including the variational approach of [13] and the Epigenetic Forest for the same floral GRN [29]—provide context. In the application (Section 6) we use the network and transition table from [18, 27]; those authors identify the fixed points (attractors) of the system and their correspondence to the genetic configurations of the floral organs (inflorescence, sepal, petal, stamen, carpel). We adopt that correspondence and add a  $p$ -adic hierarchy and an optimal gene ordering; the gene order used in the reference to write the state vector is referred to here as the *original-model ordering*. The theory rests on the existence of rational interpreters  $\phi$  and on  $\varepsilon$ -approximations in non-Archimedean fields [28]: rational functions that approximate local dynamics on disjoint balls to arbitrary precision. That construction is adapted here to GRNs, yielding approximations  $F_0, F_1, \dots, F_N$  at finitely many scales; it is because such approximations exist that we can apply  $p$ -adic fixed-point theory and the classification of ball-level dynamics.

**Contributions.** (1) A stability measure  $\mu$  on orderings and the associated notion of optimal ordering (minimizer of  $\mu$ ); (2) ball-level classification of fixed points (contracting, expanding, isometric) at each scale (Section 3), linked to  $p$ -adic fixed-point theory and the stability measure (Section 5; see also [5]); (3) an illustrative application to the *A. thaliana* Boolean model ( $N = 13$ ), where a minimizing ordering places known master regulators (UFO, EMF1, LFY, TFL1) in the leading positions and the classification distinguishes floral organs from inflorescence (e.g. IEAA vs. IEEA); (4) a companion paper [30] with further networks and basin analysis.

**Outline.** The paper is organized to build the framework from foundations to application. Section 2 recalls the  $p$ -adic numbers, ultrametric balls (Figure 2), and key fixed-point results from non-Archimedean dynamics that are used throughout. Section 3 introduces the discrete GRN model, embeds the configuration space into  $\mathbb{Z}_p$ , defines rational interpreters of the dynamics, and constructs the hierarchical approximations  $F_0, \dots, F_N$ ; it also establishes the ball-level classification (contracting, expanding, isometric) and its invariance properties. Section 4 illustrates the full construction on a small network ( $p = 2, N = 4$ ), making the definitions concrete before the general theory. Section 5 defines the stability measure  $\mu$ , proves the control identity  $\mu_E + \mu_A + \mu_I = (N-1)p^N$ , and formulates the optimization problem over orderings. Section 6 applies the framework to the *A. thaliana* floral development network ( $N = 13$ ), where the  $\mu$ -minimizing ordering places known master regulators in the leading positions and the classification separates floral organs from inflorescence. Section 7 discusses the biological and mathematical implications, compares with existing methods, identifies limitations, and summarizes the main results and Part II [30].

## Notation

Main notation used in the paper is collected in Table 1; symbols are defined in the sections indicated.

Table 1: Main notation.

Symbol	Meaning
$\mathcal{C}$	Configuration space (Section 3); $ \mathcal{C}  = p^N$ .
$N$	Number of genes (vertices).
$p$	Prime; each gene takes states in $\{0, \dots, p-1\}$ .
$\mathbb{Z}_p$	Ring of $p$ -adic integers.
$\iota$	Encoding bijection $\mathcal{C} \rightarrow \{0, \dots, p^N - 1\}$ induced by gene ordering (Section 5).
$\text{trunc}_n(a)$	$\iota(a) \bmod p^n \in \{0, \dots, p^n - 1\}$ ; index of ball containing $a$ at level $n$ .
$m_a$	Encoding $\iota(a) = \sum_{i=0}^{N-1} a_i p^i \in \{0, \dots, p^N - 1\}$ for configuration $a$ (Section 3).
$B(a)$	Ball $B_{1/p^N}(m_a) \subset \mathbb{Z}_p$ centered at $m_a$ (Section 3).
$\mathfrak{B}(a)$	Ball $\mathfrak{B}_{1/p^N}(m_a)$ in $\mathbb{C}_p$ ; $B(a) = \mathfrak{B}(a) \cap \mathbb{Z}_p$ (Section 3).
$\mathcal{U}$	Affinoid domain $\bigcup_{a \in \mathcal{C}} \mathfrak{B}(a)$ ; $\mathbb{Z}_p \subset \mathcal{U} \subset \mathfrak{B}_1(0)$ (Section 3).
$n$	Resolution level; $n \in \{0, 1, \dots, N\}$ .
$F_n$	$n$ -th rational approximation of the dynamics (Section 3).
$M_{n,m}$	Maximum common prefix length of image $p$ -adic expansions in ball $m$ at level $n$ ; $t_{n,m} = 1/p^{M_{n,m}}$ (Section 5).
$t_{n,m}$	Observable radius $1/p^{M_{n,m}}$ ; defined from $(f, \iota)$ (Section 5); equals the radius of $F_n(B_{n,m})$ when an $n$ -th approximation $F_n$ exists.
$C(n)$	Set of indices $m$ with expanding ball at level $n$ ( $t_{n,m} > 1/p^n$ ) (Section 5).
$\mu$	Stability measure $\mu_E = \sum_{n=1}^{N-1}  C(n)  \cdot p^{N-n}$ (Section 5).

## 2. Mathematical Preliminaries

We recall the  $p$ -adic foundations for our framework. For comprehensive treatments, see [5, 41, 42].

We work over the field of rational numbers  $\mathbb{Q}$ . A *non-Archimedean absolute value* on  $\mathbb{Q}$  is a map  $|\cdot| : \mathbb{Q} \rightarrow \mathbb{R}_{\geq 0}$  satisfying:

- $|x| = 0$  if and only if  $x = 0$ ,
- $|xy| = |x||y|$  for all  $x, y \in \mathbb{Q}$ , and
- the strong triangle inequality  $|x + y| \leq \max\{|x|, |y|\}$ .

The  $p$ -adic absolute values are examples of non-archimedean absolute values. A  $p$ -adic absolute value, denoted by  $|\cdot|_p$ , is defined as follows:

Fix a prime number  $p$ . For  $x \in \mathbb{Q} \setminus \{0\}$  there exists a unique  $n \in \mathbb{Z}$  and  $s, t \in \mathbb{Z}$  such that  $x = p^n \cdot \frac{s}{t}$  with  $s, t$  coprime to  $p$ , in this case we define  $|x|_p = p^{-n}$ . If  $x = 0$  we define  $|x|_p = 0$ . It is straightforward to check that this defines a non-archimedean absolute value on  $\mathbb{Q}$ . For example, with  $p = 2$  one has  $|1|_2 = 1$ ,  $|2|_2 = 1/2$ ,  $|1/2|_2 = 2$  and  $|3|_2 = 1$ .

Any such absolute value induces a *metric* by  $d(x, y) = |x - y|_p$ ; the strong triangle inequality implies that  $d$  is an *ultrametric*. For example, with this ultrametric the 2-adic distance between 1 and 3 is  $|1 - 3|_2 = |2|_2 = 1/2$ .

**Proposition 2.1** (Corollary 2.3.4 in [21]). *In the space  $(\mathbb{Q}, |\cdot|_p)$ , all triangles are isosceles.*

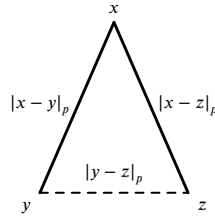
*Proof.* Let  $x, y, z \in \mathbb{Q}$ . If  $|x - y|_p = |y - z|_p$  then we are done. Hence, assume without loss of generality that  $|x - y|_p > |y - z|_p$ . Using the strong triangle inequality, on the one hand

$$|x - z|_p = |x - y + y - z|_p \leq \max\{|x - y|_p, |y - z|_p\} = |x - y|_p,$$

that is  $|x - z|_p \leq |x - y|_p$ . On the other hand

$$|x - y|_p = |x - z + z - y|_p \leq \max\{|x - z|_p, |z - y|_p\}.$$

If  $\max\{|x - z|_p, |z - y|_p\} = |z - y|_p$  then  $|x - y|_p \leq |z - y|_p < |x - y|_p$  which is a contradiction, hence  $\max\{|x - z|_p, |z - y|_p\} = |x - z|_p$ . This implies that  $|x - y|_p \leq |x - z|_p$  and therefore  $|x - z|_p = |x - y|_p$ .  $\square$



**Isosceles triangle**  
in an ultrametric:  
 $|x - y|_p = |x - z|_p \geq |y - z|_p$

Previous proposition holds in any ultrametric space, that is, a metric space  $(X, d)$  such that for all  $x, y, z \in X$ ,  $d(x, z) \leq \max\{d(x, y), d(y, z)\}$ . The *field of the p-adic numbers*  $\mathbb{Q}_p$  is the completion of  $\mathbb{Q}$  with respect to  $|\cdot|_p$ . The *ring of p-adic integers*  $\mathbb{Z}_p$  is defined by  $\mathbb{Z}_p = \{x \in \mathbb{Q}_p : |x|_p \leq 1\}$ . It is a commutative ring with unity and a subring of  $\mathbb{Q}_p$ .

Every  $x \in \mathbb{Q}_p$  has a unique expansion  $x = \sum_{i=N}^{\infty} a_i p^i$  with  $a_i \in \{0, 1, \dots, p-1\}$  (for  $x = 0$  one takes  $N = 0$ ). The usual integers  $\mathbb{Z}$  embed into  $\mathbb{Z}_p$  via base- $p$  expansion. For  $p = 2$ , the ‘‘Boolean’’ values 0 and 1 lie in  $\mathbb{Z}_2$  and  $\mathbb{Q}_2$ , which connects with the Boolean network models used in the application (Section 6).

By Ostrowski’s theorem (Theorem 3.1.3 in [21]), every non-trivial absolute value on  $\mathbb{Q}$  is equivalent to  $|\cdot|_{\infty}$  or to  $|\cdot|_p$  for some prime  $p$ ; for distinct primes  $p \neq q$ ,  $\mathbb{Q}_p \not\cong \mathbb{Q}_q$  as fields.

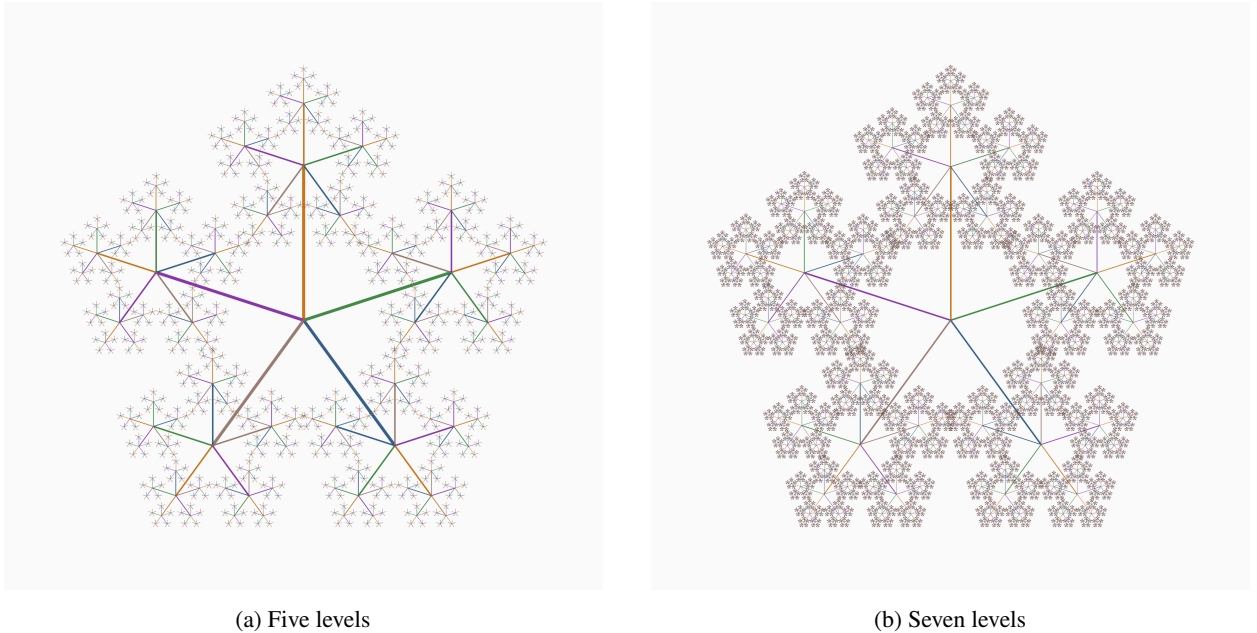


Figure 1: Fractal tree of  $\mathbb{Z}_5$  at two resolutions. Each node branches into  $p=5$  children, one per residue class; the pattern at each node reproduces the whole at a smaller scale. Points sharing a long common root-to-leaf path agree in many leading  $p$ -adic digits and are  $p$ -adically close (Remark 2.3). The branching continues identically at every scale; passing from (a) to (b) simply reveals finer detail within the same self-similar structure.

*Completions and  $\mathbb{C}_p$ .* The field  $\mathbb{Q}_p$  is complete with respect to  $|\cdot|_p$  but is not algebraically closed. Its algebraic closure  $\overline{\mathbb{Q}_p}$  is not complete. The *completion of the algebraic closure* of  $\mathbb{Q}_p$  is denoted  $\mathbb{C}_p$ ; it is complete and algebraically closed, and serves as the  $p$ -adic analogue of  $\mathbb{C}$ . The following diagram displays the completions of  $\mathbb{Q}$ ; the lower branch

represents one completion for each prime  $p$ :

$$\begin{array}{ccccc}
 & & \mathbb{R} & \xrightarrow{\text{alg. cl.}} & \mathbb{C} \\
 & \swarrow \text{compl. } |\cdot|_\infty & & & \\
 \mathbb{Z} & \hookrightarrow & \mathbb{Q} & & \\
 & \searrow \text{compl. } |\cdot|_p & & & \\
 & & \mathbb{Q}_p & \xrightarrow{\text{alg. cl.}} & \overline{\mathbb{Q}}_p \xrightarrow{\text{compl.}} \mathbb{C}_p
 \end{array} \quad (1)$$

As fields,  $\mathbb{C}_p$  and  $\mathbb{C}$  are isomorphic [21], but not as valued fields or as topological fields:  $\mathbb{C}_p$  carries the ultrametric inherited from  $\mathbb{Q}_p$ , and we work in  $\mathbb{C}_p$  so that rational functions and  $p$ -adic dynamics (e.g. fixed-point theory) are available [5].

*Topology in  $\mathbb{C}_p$ .* Notation in  $\mathbb{C}_p$  (the same definitions apply in  $\mathbb{Q}_p$  with the subscript  $p$  understood): the *closed ball* of radius  $r$  centered at  $a$  in  $\mathbb{C}_p$  is  $\mathfrak{B}_r(a) := \{x \in \mathbb{C}_p : |x-a|_p \leq r\}$ , and the *open disk* is  $\mathfrak{D}_r(a) := \{x \in \mathbb{C}_p : |x-a|_p < r\}$ .

The strong triangle inequality has several important consequences, as the following proposition shows.

**Proposition 2.2** (Proposition 2.4 in [5]).

1. Let  $a, b \in \mathbb{C}_p$  and  $s \geq r > 0$  such that  $a \in \mathfrak{B}_s(b)$ , then

$$\mathfrak{B}_r(a) \subset \mathfrak{B}_s(b) \quad \text{and} \quad \mathfrak{B}_s(a) = \mathfrak{B}_s(b).$$

That is, any point in  $\mathfrak{B}_s(b)$  is a center of the ball. The same holds for open disks.

2. Let  $\mathfrak{B}_1, \mathfrak{B}_2 \subset \mathbb{C}_p$  be two closed balls (or open disks) such that  $\mathfrak{B}_1 \cap \mathfrak{B}_2 \neq \emptyset$ , then

$$\text{either } \mathfrak{B}_1 \subset \mathfrak{B}_2 \quad \text{or} \quad \mathfrak{B}_2 \subset \mathfrak{B}_1.$$

That is, either two balls are disjoint or one contains the other. The same holds for open disks.

3. All closed balls and open disks in  $\mathbb{C}_p$  are both open and closed (clopen) topologically.

4.  $\mathbb{C}_p$  is totally disconnected as a topological space.

The equivalent statements remain true for any ultrametric space.

*Proof.*

1. Since  $a \in \mathfrak{B}_s(b)$ , we have  $|a-b|_p \leq s$ . Let  $x \in \mathfrak{B}_r(a)$ , then  $|x-a|_p \leq r \leq s$ . By strong triangle inequality

$$|x-b|_p = |x-a+a-b|_p \leq \max\{|x-a|_p, |a-b|_p\} \leq s,$$

and hence  $x \in \mathfrak{B}_s(b)$ . Thus  $\mathfrak{B}_r(a) \subset \mathfrak{B}_s(b)$ . The reverse inclusion when  $r = s$  is similar. A similar proof holds for open disks.

2. Without loss of generality, assume that the radius of  $\mathfrak{B}_2$  is greater than or equal to the radius of  $\mathfrak{B}_1$ . Let  $a \in \mathfrak{B}_1 \cap \mathfrak{B}_2$ . By part 1 we have that  $\mathfrak{B}_1 \subset \mathfrak{B}_2$ .

3. Let  $\mathfrak{B}_s(a) \subset \mathbb{C}_p$  be a closed ball and let  $x \in \mathfrak{B}_s(a)$ . Choose  $0 < r < s$ . Then by part 1,

$$\mathfrak{D}_r(x) \subset \mathfrak{B}_r(x) \subset \mathfrak{B}_s(a).$$

Hence,  $\mathfrak{B}_s(a)$  is open in the topology.

On the other hand. Let  $\mathfrak{D} := \mathbb{C}_p \setminus \mathfrak{B}_s(a)$  and let  $x \in \mathfrak{D}$ . Then  $x \notin \mathfrak{B}_s(a)$ . Choose  $0 < r < s$ . By part 2,

$$\mathfrak{B}_r(x) \cap \mathfrak{B}_s(a) = \emptyset$$

since otherwise  $x \in \mathfrak{B}_s(a)$ . This implies that

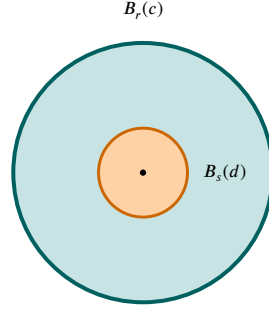
$$\mathfrak{D}_r(x) \subset \mathfrak{B}_r(x) \subset \mathfrak{D}.$$

Therefore,  $\mathfrak{D}$  is open, which implies that  $\mathfrak{B}_s(a)$  is closed in the topology. A similar proof holds for open disks.

4. Let  $X \subset \mathbb{C}_p$  be a subset with at least two distinct elements  $x, y \in X$ . Choose  $r$  such that  $0 < r < |x - y|_p$ . Then  $\mathfrak{B} := \mathfrak{B}_r(x)$  and  $\mathfrak{D} := \mathbb{C}_p \setminus \mathfrak{B}_r(x)$  are two disjoint open sets such that

$$\mathfrak{D} \cap \mathfrak{B} = \emptyset, \quad \mathfrak{D} \cap X \neq \emptyset, \quad \mathfrak{B} \cap X \neq \emptyset, \quad \text{and} \quad X \subset \mathfrak{D} \cup \mathfrak{B}.$$

Therefore,  $X$  is disconnected. As  $X$  was arbitrary we conclude that  $\mathbb{C}_p$  is totally disconnected. □



**Intersecting balls**  
one contains the other;  
any point in the intersection is a center

Figure 2: Ultrametric property: two intersecting balls in  $\mathbb{C}_p$  share a point  $z$ ; recentering at  $z$  shows one ball is contained in the other. The isosceles property of ultrametric triangles is illustrated inline in the text.

For  $a \in \mathbb{Z}_p$ , the intersection  $\mathfrak{B}_r(a) \cap \mathbb{Z}_p$  is a closed ball in  $\mathbb{Z}_p$ ; we denote it  $B_r(a) := \mathfrak{B}_r(a) \cap \mathbb{Z}_p$ . In particular  $\mathbb{Z}_p = \mathfrak{B}_1(0) \cap \mathbb{Q}_p$ . The *diameter* of a set  $S$  is  $\text{diam}(S) := \sup\{|x - y|_p : x, y \in S\}$ ; in an ultrametric space the diameter of a closed ball equals its radius.

**Remark 2.3** (Hierarchical Partition and Nested Balls). *We call  $B_r(a)$  the “observable” ball when  $a \in \mathbb{Z}_p$  (it equals  $\mathfrak{B}_r(a) \cap \mathbb{Z}_p$  by the notation above; if  $a \notin \mathbb{Z}_p$  and  $\mathfrak{B}_r(a) \cap \mathbb{Z}_p \neq \emptyset$ , then by the ultrametric property there exists  $b \in \mathbb{Z}_p$  with  $\mathfrak{B}_r(a) \cap \mathbb{Z}_p = B_r(b)$ ). For any  $x \in \mathbb{Z}_p$  and  $n \geq 1$ , there exists a unique  $m \in \{0, \dots, p^n - 1\}$  such that  $x \in B_{1/p^n}(m)$ , where  $m = \alpha_0 + \alpha_1 p + \dots + \alpha_{n-1} p^{n-1}$  corresponds to the first  $n$  terms of the  $p$ -adic expansion of  $x$ . Thus:*

$$B_{1/p^n}(m) = \{x \in \mathbb{Z}_p : x = m + p^n y, y \in \mathbb{Z}_p\}.$$

*This gives a hierarchical partition of  $\mathbb{Z}_p$ : balls at finer scales nest within coarser balls; each  $B_{1/p^n}(m)$  is the disjoint union of  $p$  sub-balls  $B_{1/p^{n+1}}(m + kp^n)$ ,  $k = 0, \dots, p - 1$ . Any two balls are either disjoint or one contains the other (or equal if same radius; see Figure 3).*

**Lemma 2.4** (Ball-truncation equivalence). *For each  $n \geq 1$  and  $m \in \{0, \dots, p^n - 1\}$ , the ball  $B_{1/p^n}(m)$  consists of exactly those  $x \in \mathbb{Z}_p$  whose  $p$ -adic expansion agrees with  $m$  in the first  $n$  digits (i.e.,  $x \equiv m \pmod{p^n}$ ). Hence  $B_{1/p^n}(m)$  has normalized Haar measure  $p^{-n}$  (see e.g. [41]).*

*Proof.* The equality  $B_{1/p^n}(m) = \{x \in \mathbb{Z}_p : x \equiv m \pmod{p^n}\}$  is the content of the  $p$ -adic expansion and the definition of the ball. The normalized Haar measure of this ball is  $p^{-n}$ . □

### Hierarchical p-adic framework for GRNs

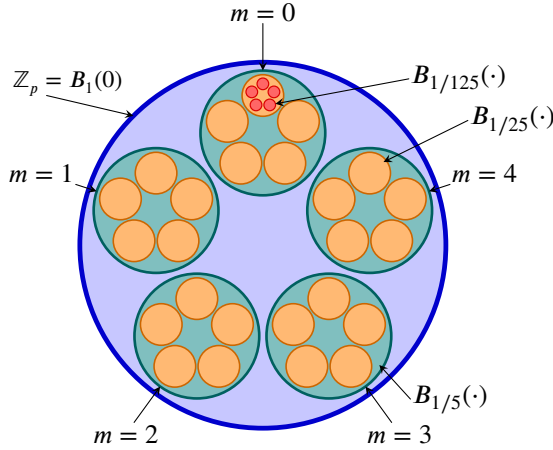


Figure 3: Hierarchical partition of  $\mathbb{Z}_p$  for  $p = 5$ . The ball  $\mathbb{Z}_p = B_1(0)$  is the disjoint union of five balls  $B_{1/5}(m)$ ,  $m = 0, \dots, 4$  (radius  $1/5$ , level 1). Each is subdivided into five balls of radius  $1/25$  (level 2); inside the ball  $m = 0$  (i.e.  $B_{1/25}(0)$  at level 2), one of those is further subdivided into five balls of radius  $1/125$  (level 3). The same pattern repeats at every scale.

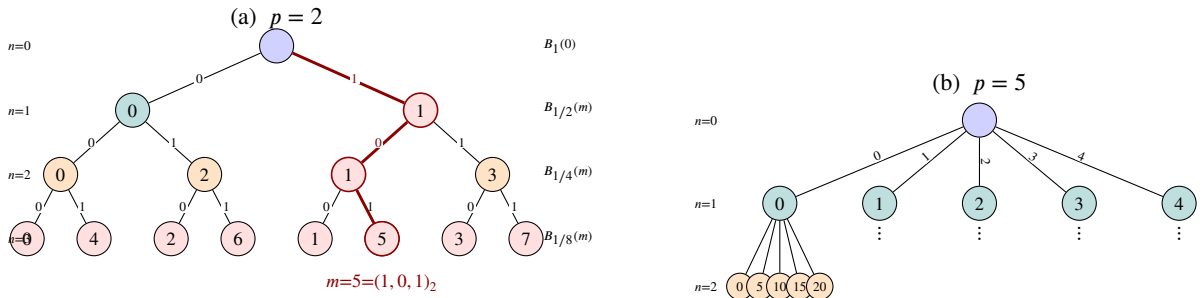


Figure 4: Tree representation of  $\mathbb{Z}_p$ . Each node at depth  $n$  corresponds to a ball  $B_{1/p^n}(m)$ ; its  $p$  children are the sub-balls at level  $n+1$ . Edge labels indicate the  $n$ -th digit  $a_n \in \{0, \dots, p-1\}$ ; a root-to-leaf path encodes the  $p$ -adic expansion of a configuration. (a)  $\mathbb{Z}_2$ , levels  $n=0-3$ ; the highlighted path traces  $m = 5 = (1, 0, 1)_2$ . (b)  $\mathbb{Z}_5$ , levels  $n=0-1$ , with one branch expanded to  $n=2$ ; the remaining branches subdivide identically. Compare with the spatial (nested-ball) view in Figure 3.

*Rational functions, dynamics, and approximation.* The projective line over  $\mathbb{C}_p$  is  $\mathbb{P}^1(\mathbb{C}_p) = \mathbb{C}_p \cup \{\infty\}$ , i.e.,  $\mathbb{C}_p$  with one point at infinity adjoined (formally: the set of equivalence classes  $[z : w]$  with  $(z, w) \in \mathbb{C}_p^2 \setminus \{(0, 0)\}$  under  $(z, w) \sim (\lambda z, \lambda w)$  with  $\lambda \neq 0$ ; we identify  $\mathbb{C}_p$  with  $[z : 1]$  and  $\infty$  with  $[1 : 0]$ ). A ball in  $\mathbb{P}^1(\mathbb{C}_p)$  is either a closed ball in  $\mathbb{C}_p$  (as defined above) or the complement in  $\mathbb{P}^1(\mathbb{C}_p)$  of an open disk in  $\mathbb{C}_p$ —i.e., a set of the form  $\mathbb{P}^1(\mathbb{C}_p) \setminus \mathfrak{D}_r(a)$ , which is a neighborhood of  $\infty$ . Thus the balls in  $\mathbb{P}^1(\mathbb{C}_p)$  are exactly the images of closed balls in  $\mathbb{C}_p$  under the Möbius transformations that identify charts around  $\infty$ . Open disks in  $\mathbb{P}^1(\mathbb{C}_p)$  are defined analogously.

Let  $\phi \in \mathbb{C}_p(z)$  be a rational function. A key result is:

**Proposition 2.5** (Proposition 3.25 in [5]). *Let  $\mathfrak{B}$  be a ball in  $\mathbb{C}_p$  and  $\phi \in \mathbb{C}_p(z)$  nonconstant. Then  $\phi(\mathfrak{B})$  is either  $\mathbb{P}^1(\mathbb{C}_p)$  or a ball in  $\mathbb{P}^1(\mathbb{C}_p)$ .*

Thus rational functions map balls to balls (in  $\mathbb{P}^1(\mathbb{C}_p)$ ); this underlies the interpretation of discrete dynamics in Section 3.

A point  $x$  is a *fixed point* if  $\phi(x) = x$ . The *multiplier*  $\lambda = \phi'(x)$  classifies  $x$  as:

- *Attracting* if  $|\lambda|_p < 1$

- *Repelling* if  $|\lambda|_p > 1$
- *Indifferent* if  $|\lambda|_p = 1$

**Remark 2.6** (Terminology). *In the discrete-dynamics and Boolean-network literature, configurations  $a$  with  $f(a) = a$  are often called “attractors” or “stable states.” We reserve fixed point for that combinatorial notion and use attracting/repelling/indifferent exclusively for the multiplier classification above.*

The ball-level analogue (contracting/expanding/isometric) is introduced in Definition 3.16.

**Proposition 2.7** (Theorem 4.18 in [5]). *Let  $U = \mathfrak{D}_r(a)$  and  $\phi \in \mathbb{C}_p(z)$  with  $\phi(U)$  a disk.*

- If  $\phi(U) \subsetneq U$ , there is a unique attracting fixed point in  $U$ . (In  $p$ -adic dynamics this strict inclusion plays the role of a contraction: it implies that iterates converge to the fixed point; no separate metric contraction hypothesis is required.)*
- If  $\phi(U) \supsetneq U$  and  $\phi$  has Weierstrass degree 1 on  $U$ , then  $\phi$  is one-to-one on  $U$  and there is a unique repelling fixed point in  $U$  (see [5, Theorem 3.13]).*
- If  $\phi : U \rightarrow U$  is bijective, any fixed points in  $U$  are indifferent.*

The ball-level analogue of this classification is given in Definition 3.16 (Section 3).

*$\varepsilon$ -Approximations.* The following theorem from [28] is fundamental to the construction in Section 3: it provides a “gluing” technique that builds a global rational function from prescribed local dynamics on disjoint balls.

**Theorem 2.8** ( $\varepsilon$ -approximation; Theorem 4.2 in [28]). *Let  $\phi_1, \dots, \phi_n \in \mathbb{C}_p(z)$  and let  $B := \bigcup_{i=1}^n \mathfrak{B}_{r_i}(a_i)$  be a union of pairwise disjoint closed balls in  $\mathbb{C}_p$ . Suppose that  $\phi_i(\mathfrak{B}_{r_i}(a_i)) = \mathfrak{B}_{r_i}(b_i)$  for each  $i$ , and that  $\phi_i(B) \subset \mathfrak{B}_1(0)$  for all  $i = 1, \dots, n$ . Then for any  $\varepsilon > 0$  there exists  $F_\varepsilon \in \mathbb{C}_p(z)$  such that:*

- $F_\varepsilon(\mathfrak{B}_{r_i}(a_i)) = \mathfrak{B}_{r_i}(b_i)$  for each  $i$  (the image of each input ball equals the prescribed target ball in  $\mathbb{C}_p$ ),
- $|F_\varepsilon(z) - \phi_i(z)|_p < \varepsilon$  for all  $z \in \mathfrak{B}_{r_i}(a_i)$ .

One explicit construction is  $F_\varepsilon(z) = \sum_i \phi_i(z)h_i(z)$  with  $h_i(z) = (1 - ((z - a_i)/c_i)^{M_i})^{-1}$  for appropriate  $c_i, M_i$ . This “gluing” technique enables constructing global rational functions from local dynamics on disjoint balls; details are given therein. Main notation is collected in Table 1 (Section 1).

### 3. Hierarchical $p$ -Adic Ball Dynamics for Gene Regulatory Networks

GRNs model interactions among genes and regulators and are central to understanding cell differentiation, morphogenesis, and adaptive responses. In this paper they are treated as discrete dynamical systems: each configuration is a state, and the dynamics are given by a map  $f$ . The configuration space  $\mathcal{C}$  is embedded into  $\mathbb{Z}_p$  as a collection of ultrametric balls, and the fractal structure of  $\mathbb{Z}_p$  (nested balls at scales  $1/p^n$ ; see Figure 1) is used to model the dynamics via rational approximations  $F_0, F_1, \dots, F_N$ , each capturing behavior at one scale.

Let  $p$  be prime and consider a GRN with  $N$  vertices  $x_0, \dots, x_{N-1}$ , each with states in  $\{0, \dots, p-1\}$ . A *configuration* is a choice of state per vertex; the *configuration space* has  $p^N$  elements:

$$\mathcal{C} = \{(a_0, a_1, \dots, a_{N-1}) \mid a_i \in \{0, 1, \dots, p-1\} \text{ for all } i\}. \quad (2)$$

The GRN defines a *discrete dynamical system*  $f : \mathcal{C} \rightarrow \mathcal{C}$ , as in Boolean and logical models [2, 8, 11, 14, 20, 25–27]. We study iterates  $f^n$  and long-term behavior: attractors, repelling states, and periodic points.

*Embedding Configurations as  $p$ -Adic Balls.* Extending the discrete dynamics  $f$  to a continuous setting requires care. Polynomial interpolation over finite fields, for instance, involves  $p^N$  coefficients, is far from unique, and the resulting high-degree maps offer little control over the dynamics—they can create fixed points or attractors absent from the original system. The  $p$ -adic integers offer a natural alternative [5, 17, 39] that:

- Respects the hierarchical structure of regulatory interactions,
- Provides a natural multi-scale analysis,
- Enables controlled approximation of dynamics,
- Reveals latent stability patterns not evident in flat combinatorial models.

These properties are developed below and in Section 5; Theorem 2.8 provides the approximation tool.

We embed  $C$  into  $\mathbb{Z}_p$  as follows. To each  $a = (a_0, \dots, a_{N-1}) \in C$  associate the integer

$$m_a = \sum_{i=0}^{N-1} a_i p^i, \quad (3)$$

and then map  $a$  to the closed ball:

$$B(a) := B_{1/p^N}(m_a). \quad (4)$$

Then  $\mathbb{Z}_p = \bigsqcup_{a \in C} B(a)$  (disjoint union; Figure 3):  $p^N$  balls of radius  $1/p^N$ , one per configuration. Under this embedding, each ball  $B_{1/p^n}(m_a)$  (Lemma 2.4) therefore contains exactly  $p^{N-n}$  configuration balls of radius  $1/p^N$ . The expansion (3) encodes hierarchy: genes at lower powers of  $p$  have greater influence on  $p$ -adic distance.

*Interpreting Discrete Dynamics in  $p$ -Adic Space.* Denote  $\mathfrak{B}(a) := \mathfrak{B}_{1/p^N}(m_a)$  the corresponding ball in  $\mathbb{C}_p$ ; then  $\mathfrak{B}(a) \cap \mathbb{Z}_p = B(a)$ . The *affinoid domain* associated to  $C$  is  $\mathcal{U} := \bigcup_{a \in C} \mathfrak{B}(a)$ ; it is a finite disjoint union of closed balls in  $\mathbb{C}_p$  satisfying  $\mathbb{Z}_p \subset \mathcal{U} \subset \mathfrak{B}_1(0)$ . (In rigid geometry, affinoid domains are certain compact subsets of  $\mathbb{C}_p$ ; here we only need that  $\mathcal{U}$  is a finite disjoint union of closed balls, and we keep the name for consistency with the literature.) The *projection*  $\pi : \mathcal{U} \rightarrow C$  sends each  $x \in \mathcal{U}$  to the unique  $a \in C$  such that  $x \in \mathfrak{B}(a)$ .

**Definition 3.1.** Let  $\phi \in \mathbb{C}_p(z)$  be a rational function. We say that  $\phi$  interprets the dynamics of  $f$  if

$$\phi(\mathfrak{B}(a)) \subseteq \mathfrak{B}(f(a)) \quad \text{for all } a \in C.$$

Equivalently,  $\phi$  maps  $\mathcal{U}$  to itself and the following diagram commutes:

$$\begin{array}{ccc} \mathcal{U} & \xrightarrow{\phi} & \mathcal{U} \\ \pi \downarrow & & \downarrow \pi \\ C & \xrightarrow{f} & C \end{array}$$

Since each  $\mathfrak{B}(a)$  is clopen in  $\mathcal{U}$ , the map  $\pi$  is continuous (in fact locally constant) when  $C$  carries the discrete topology. In the language of topological dynamics,  $\pi$  is a *semi-conjugacy* from  $(\mathcal{U}, \phi)$  to  $(C, f)$ ; in particular, it preserves periodic orbits and maps attracting structures of  $\phi$  to those of  $f$ .

**Remark 3.2** (Observational semantics). *The clopen balls  $\mathfrak{B}(a)$  can be regarded as finest-resolution observables: the statement “the system is in configuration  $a$ ” is represented by membership in  $\mathfrak{B}(a)$ . More generally, unions of such balls represent coarse-grained observables. Under this reading, the semi-conjugacy  $\pi$  expresses that the rational interpreter  $\phi$  preserves the finite update rule not only on individual configurations, but on observable classes of states.*

**Corollary 3.3** (of Theorem 2.8; existence of rational interpreters). *For any  $f : C \rightarrow C$  with the embedding of Section 3, there exists  $\phi \in \mathbb{C}_p(z)$  such that  $\phi(\mathfrak{B}(a)) = \mathfrak{B}(f(a))$  for all  $a \in C$ .*

*Proof.* For each  $a \in C$ , define  $g_a(z) = A_a(z - m_a) + m_{f(a)}$  with  $|A_a|_p = 1$ ; then  $g_a(\mathfrak{B}(a)) = \mathfrak{B}(f(a))$ . We verify the hypotheses of Theorem 2.8: the balls  $\{\mathfrak{B}(a)\}_{a \in C}$  are pairwise disjoint (Section 3), each  $g_a$  maps its ball onto the prescribed target, and  $g_a(\mathcal{U}) \subset \mathfrak{B}_1(0)$  because  $\mathcal{U} \subset \mathfrak{B}_1(0)$  and  $|A_a|_p = 1$ . Theorem 2.8 yields  $\phi \in \mathbb{C}_p(z)$  with  $\phi(\mathfrak{B}(a)) = \mathfrak{B}(f(a))$  for all  $a$ .  $\square$

**Remark 3.4** (Interpreter: non-uniqueness and role). *From the proof of Corollary 3.3 it follows that the interpreter  $\phi$  is not unique, and from Theorem 2.8 we can see that its degree is not optimal. Although the inclusion  $\phi(\mathfrak{B}(a)) \subseteq \mathfrak{B}(f(a))$  suffices for our purposes, the same corollary allows us to assume that  $\phi(\mathfrak{B}(a)) = \mathfrak{B}(f(a))$ .*

*Despite  $\phi$  can be constructed explicitly via the gluing technique of [28], its explicit form is not needed for computation—all practical quantities depend only on  $(f, \iota)$  (Theorem 5.5)—but its existence, guaranteed by the construction over  $\mathbb{C}_p$  (Corollary 3.3), is essential for the mathematical justification of the ball-level classification (Definition 3.16).*

**Hierarchical Rational Approximations.** Let  $\phi \in \mathbb{C}_p(z)$  interpret  $f$ . We construct approximations  $F_0, \dots, F_N \in \mathbb{C}_p(z)$  with  $|F_n(z) - \phi(z)|_p \leq 1/p^m$  for some  $m \in \{0, \dots, N\}$  and all  $z \in \mathbb{Z}_p$  (Proposition 3.11); in particular  $|F_N(z) - \phi(z)|_p \leq 1/p^N$ . The  $F_n$  yield stability and periodic structure (Section 3).

For  $n \geq 0$ ,  $\mathbb{Z}_p = \bigsqcup_{m=0}^{p^n-1} B_{1/p^n}(m)$ ; write  $B_{n,m} := B_{1/p^n}(m) \subset \mathbb{Z}_p$ , so  $B_{N,m} = B(m) = B_{1/p^N}(m)$ . Each  $a \in C$  has  $m = \sum_{i=0}^{N-1} a_i p^i$ ,  $\mathfrak{B}(a) = \mathfrak{B}_{1/p^N}(m)$ , and  $B(a) = B_{1/p^N}(m)$ .

For each ball  $B_{n,m}$ , we define

$$t_{n,m} = \max \left( \{1/p^N\} \cup \{|\phi(x) - \phi(y)|_p : x, y \in B_{n,m}\} \right); \quad (5)$$

when an interpreter  $\phi$  exists and has no poles in  $B_{n,m}$ , this is the diameter of the image of  $B_{n,m}$  under  $\phi$ ; in our construction (Section 3) the interpreters are affine on each  $\mathfrak{B}(a)$ , so this holds for the balls we use. Thus  $t_{n,m}$  measures the output resolution associated to the input observable  $B_{n,m}$ : it records how far the images of states that are indistinguishable at level  $n$  can separate after one update, quantifying expansion or concentration of observational uncertainty.

**Remark 3.5** (Computation of  $t_{n,m}$  from Discrete Data). *The values  $t_{n,m}$  can be computed directly from the discrete transition data  $f : C \rightarrow C$ . This follows from:*

1. *For any configuration  $a \in C$  with  $\mathfrak{B}(a) \subset B_{n,m}$ , the image  $\phi(\mathfrak{B}(a))$  is contained in  $\mathfrak{B}(f(a))$ , and the target ball is determined by the discrete dynamics  $f(a)$ .*
2. *The p-adic distance  $|\phi(x) - \phi(y)|_p$  for  $x \in \mathfrak{B}(a)$  and  $y \in \mathfrak{B}(b)$  (with  $a, b \in C$ ) depends only on the first differing digit between  $f(a)$  and  $f(b)$ :*

$$|\phi(x) - \phi(y)|_p = \begin{cases} \leq 1/p^N & \text{if } f(a) = f(b), \\ 1/p^j & \text{if } f(a) \neq f(b), \text{ and } j \text{ is the first differing position.} \end{cases} \quad (6)$$

3. *Therefore,  $t_{n,m}$  can be computed algorithmically as follows:*

- (a) *Enumerate all configurations  $a \in C$  with  $\mathfrak{B}(a) \subset B_{n,m}$ .*
- (b) *Compute images  $f(a)$  and integers  $m_{f(a)} = \sum_{i=0}^{N-1} (f(a))_i p^i$ .*
- (c) *Set  $t_{n,m} = \max(\{1/p^N\} \cup \{m_{f(a)} - m_{f(b)}\}_p : \mathfrak{B}(a), \mathfrak{B}(b) \subset B_{n,m})$ .*

**Lemma 3.6.**  $t_{n,m} = 1/p^M$  for some  $M \in \{0, 1, \dots, N\}$ .

*Proof.* By Remark 3.5,  $t_{n,m}$  is the maximum of  $1/p^N$  and finitely many values of the form  $|m_{f(a)} - m_{f(b)}|_p$  with  $\mathfrak{B}(a), \mathfrak{B}(b) \subset B_{n,m}$ ; each such value is  $1/p^j$  for some  $j \in \{0, \dots, N\}$ . Hence  $t_{n,m} = 1/p^M$  for some  $M \in \{0, 1, \dots, N\}$ .  $\square$

**Lemma 3.7** (Monotonicity of  $t_{n,m}$ ). *If  $B_{1/p^{n+1}}(m') \subseteq B_{1/p^n}(m)$ , then  $t_{n+1,m'} \leq t_{n,m}$ .*

*Proof.* By equation (5),  $t_{n,m} = \max(\{1/p^N\} \cup \{|\phi(x) - \phi(y)|_p : x, y \in B_{n,m}\})$  and  $t_{n+1,m'} = \max(\{1/p^N\} \cup \{|\phi(x) - \phi(y)|_p : x, y \in B_{n+1,m'}\})$ . Since  $B_{n+1,m'} \subseteq B_{n,m}$ , every pair  $(x, y)$  in  $B_{n+1,m'}$  lies in  $B_{n,m}$ , so the set over which the maximum is taken for  $t_{n+1,m'}$  is contained in the set for  $t_{n,m}$ . Hence  $t_{n+1,m'} \leq t_{n,m}$ .  $\square$

**Definition 3.8.** *We define an n-th approximation of  $f$  as a rational function  $F_n \in \mathbb{C}_p(z)$  such that  $F_n(\mathfrak{B}_{1/p^n}(m)) = \mathfrak{B}_{t_{n,m}}(\phi(m))$ .*

$\mathfrak{B}_{t_{n,m}}(\phi(m))$  is the smallest closed ball in  $\mathbb{C}_p$  that contains all the images  $\phi(z)$  for  $z \in B_{n,m}$ . The existence of such approximations is guaranteed by the following theorem, which is a direct application of Theorem 2.8 from [28].

**Proposition 3.9** (Existence of Hierarchical Approximations). *Let  $f : C \rightarrow C$  be a discrete dynamical system, and let  $\phi \in \mathbb{C}_p(z)$  be a rational function that interprets the dynamics of  $f$ . For each resolution level  $n \in \{0, \dots, N\}$ , there exists a rational function  $F_n \in \mathbb{C}_p(z)$  that satisfies the mapping property:*

$$F_n(\mathfrak{B}_{1/p^n}(m)) = \mathfrak{B}_{t_{n,m}}(\phi(m)) \quad \text{for each } m \in \{0, \dots, p^n - 1\}, \quad (7)$$

where  $t_{n,m}$  is defined as in equation (5).

*Proof.* It follows from a similar argument to the proof of Corollary 3.3. □

This yields a finite sequence  $F_0, F_1, \dots, F_N$  with the mapping property (7); the uniform approximation on  $\mathbb{Z}_p$  is given by Proposition 3.11 below. Non-uniqueness and invariance of classification are in Proposition 3.12 and Section 5.

At each resolution  $n$ , the partition  $\mathbb{Z}_p = \bigsqcup_m B_{1/p^n}(m)$  groups configurations that share the same first  $n$  digits (Section 3); the gene ordering determines which configurations are “close” at each scale. The classification of a ball as  $n$ -contracting or  $n$ -expanding (Definition 3.16) depends on this grouping; refinement from  $F_n$  to  $F_{n+1}$  can reveal sub-balls with different stability. Different orderings yield different approximations and classifications (Remark 3.18). In particular, the value  $t_{n,m}$  captures the dynamical spread within  $B_{1/p^n}(m)$ : if all configurations in the ball map to the same configuration,  $t_{n,m} = 1/p^N$  (high stability); if they map to different configurations, then  $t_{n,m} > 1/p^N$  and genes at lower  $p$ -adic positions contribute more to the separation, reflecting their greater hierarchical influence.

*Properties of the Approximation Sequence.* The sequence  $\{F_n\}$  satisfies consistency (Proposition 3.10), approximation to  $\phi$  along the finite refinement (Proposition 3.11), and invariance under small perturbations (Proposition 3.12, Corollary 3.13).

**Proposition 3.10.** *Let  $F_n, F_{n+1}$  be two approximations with  $0 \leq n < n+1 \leq N$ . Let us assume that  $F_n(\mathfrak{B}_{1/p^n}(m)) = \mathfrak{B}_{1/p^M}(\phi(m))$  for some  $m \in \{0, 1, \dots, p^n - 1\}$  and some  $M \in \{0, 1, \dots, N\}$ , then:*

$$|F_n(z) - F_{n+1}(z)|_p \leq \frac{1}{p^M} \quad \text{for all } z \in B_{1/p^n}(m). \quad (8)$$

*Proof.* Let  $z \in B_{1/p^n}(m)$ , then by hypothesis  $F_n(z) \in \mathfrak{B}_{1/p^M}(\phi(m))$ , which implies that  $|F_n(z) - \phi(m)|_p \leq \frac{1}{p^M}$ .

Since  $z \in B_{1/p^n}(m)$  then there exists a configuration  $a \in C$  and an integer  $m_2 \in \{0, 1, \dots, p^{n+1} - 1\}$  such that  $z \in \mathfrak{B}(a) \subset \mathfrak{B}_{1/p^{n+1}}(m_2) \subset \mathfrak{B}_{1/p^n}(m)$ .

By definition,  $F_{n+1}(\mathfrak{B}_{1/p^{n+1}}(m_2)) = \mathfrak{B}_{t_{n+1,m_2}}(\phi(m_2))$ , which implies that  $F_{n+1}(z) \in \mathfrak{B}_{t_{n+1,m_2}}(\phi(m_2))$  and hence  $|F_{n+1}(z) - \phi(m_2)|_p \leq t_{n+1,m_2}$ .

Since  $m_2 \in \mathfrak{B}_{1/p^n}(m)$  and  $\phi$  maps  $\mathfrak{B}_{1/p^n}(m)$  into  $\mathfrak{B}_{t_{n,m}}(\phi(m)) = \mathfrak{B}_{1/p^M}(\phi(m))$ , we have  $|\phi(m_2) - \phi(m)|_p \leq \frac{1}{p^M}$ , i.e.,  $\phi(m_2) \in \mathfrak{B}_{1/p^M}(\phi(m))$ . By Lemma 3.7, since  $\mathfrak{B}_{1/p^{n+1}}(m_2) \subset \mathfrak{B}_{1/p^n}(m)$ , we have  $t_{n+1,m_2} \leq t_{n,m} = 1/p^M$ . The ultrametric property then gives  $\mathfrak{B}_{t_{n+1,m_2}}(\phi(m_2)) \subseteq \mathfrak{B}_{1/p^M}(\phi(m_2)) \subseteq \mathfrak{B}_{1/p^M}(\phi(m))$ .

Finally, using the ultrametric inequality:

$$\begin{aligned} |F_n(z) - F_{n+1}(z)|_p &= |F_n(z) - \phi(m) + \phi(m) - \phi(m_2) + \phi(m_2) - F_{n+1}(z)|_p \\ &\leq \max\{|F_n(z) - \phi(m)|_p, |\phi(m_2) - \phi(m)|_p, |F_{n+1}(z) - \phi(m_2)|_p\} \\ &\leq \frac{1}{p^M}. \end{aligned} \quad (9)$$

□

The rational functions  $F_n$  approximate  $\phi$  along the finite refinement (as  $n$  increases toward the final resolution  $N$ ), in the following precise sense.

**Proposition 3.11.** *Let  $\phi$  interpret  $f$  and let  $F_n$  be the  $n$ -th approximation. For each ball  $B_{n,m} = \mathfrak{B}_{1/p^n}(m) \cap \mathbb{Z}_p$ , if  $F_n(\mathfrak{B}_{1/p^n}(m)) = \mathfrak{B}_{1/p^M}(\beta)$  for some  $M \leq N$ , then*

$$|\phi(z) - F_n(z)|_p \leq \frac{1}{p^M} \quad \text{for all } z \in B_{n,m}.$$

*Proof.* By hypothesis,  $F_n(z) \in \mathfrak{B}_{1/p^M}(\beta)$  for every  $z \in \mathfrak{B}_{1/p^n}(m)$ . We show that  $\phi(z)$  lies in the same ball. Since  $\phi$  interprets  $f$ , for each configuration  $a$  with  $m_a \in B_{n,m}$  we have  $\phi(\mathfrak{B}(a)) \subseteq \mathfrak{B}(f(a))$ ; because  $t_{n,m} = 1/p^M$ , all image balls  $\mathfrak{B}(f(a))$  lie in  $\mathfrak{B}_{1/p^M}(\beta)$ , so  $\phi(z) \in \mathfrak{B}_{1/p^M}(\beta)$  for all  $z \in B_{n,m}$ . Since both  $\phi(z)$  and  $F_n(z)$  belong to  $\mathfrak{B}_{1/p^M}(\beta)$ , the ultrametric inequality gives  $|\phi(z) - F_n(z)|_p \leq 1/p^M$ .  $\square$

**Proposition 3.12.** *Let  $F_n \in \mathbb{C}_p(z)$  be an  $n$ -th approximation. Let us assume that  $\hat{M} = \max_{0 \leq m \leq p^n - 1} \{M : F_n(\mathfrak{B}_{1/p^n}(m)) = \mathfrak{B}_{1/p^M}(\phi(m))\}$ . Let  $h \in \mathbb{C}_p(z)$  be a rational function such that:*

$$|h(z)|_p < \frac{1}{p^{\hat{M}}}, \quad \text{for all } z \in \bigsqcup_{m=0}^{p^n-1} \mathfrak{B}_{1/p^n}(m). \quad (10)$$

Then  $F'_n := F_n + h \in \mathbb{C}_p(z)$  is also an  $n$ -th approximation.

*Proof.* It is sufficient to prove that  $F'_n(\mathfrak{B}_{1/p^n}(m)) = F_n(\mathfrak{B}_{1/p^n}(m))$  for all  $m = 0, \dots, p^n - 1$ .

Let  $m \in \{0, \dots, p^n - 1\}$  and let us assume that  $F_n(\mathfrak{B}_{1/p^n}(m)) = \mathfrak{B}_{1/p^M}(\phi(m))$  for some  $M \in \{0, 1, \dots, N\}$ . By hypothesis  $\hat{M} \geq M$ , therefore  $1/p^{\hat{M}} \leq 1/p^M$  and for all  $z \in \mathfrak{B}_{1/p^n}(m)$ :

$$\begin{aligned} |F'_n(z) - \phi(m)|_p &= |F'_n(z) - F_n(z) + F_n(z) - \phi(m)|_p \\ &= |h(z) + F_n(z) - \phi(m)|_p \\ &\leq \max\{|h(z)|_p, |F_n(z) - \phi(m)|_p\} \leq \frac{1}{p^M}. \end{aligned} \quad (11)$$

hence  $F'_n(\mathfrak{B}_{1/p^n}(m)) \subset \mathfrak{B}_{1/p^M}(\phi(m))$ .

To show equality, note that since  $|h(z)|_p < 1/p^{\hat{M}} \leq 1/p^M$  and  $F_n(\mathfrak{B}_{1/p^n}(m)) = \mathfrak{B}_{1/p^M}(\phi(m))$ , there exists  $z_0 \in \mathfrak{B}_{1/p^n}(m)$  such that  $|F_n(z_0) - \phi(m)|_p = \frac{1}{p^M}$ . For such  $z_0$ , we have  $|F'_n(z_0) - \phi(m)|_p = \frac{1}{p^M}$  (since  $|h(z_0)|_p < 1/p^M$  cannot cancel the maximum), therefore  $F'_n(\mathfrak{B}_{1/p^n}(m)) = \mathfrak{B}_{1/p^M}(\phi(m))$ .  $\square$

**Corollary 3.13** (Invariance of Expanding Classification Under Perturbation). *Let  $F_n$  and  $F'_n = F_n + h$  be two  $n$ -th approximations as in Proposition 3.12. For each ball  $B_{1/p^n}(m)$ , the classification as expanding (i.e., whether  $\text{diam}(F_n(B_{1/p^n}(m))) > 1/p^n$ ) is preserved:*

$$\text{diam}(F_n(B_{1/p^n}(m))) > \frac{1}{p^n} \iff \text{diam}(F'_n(B_{1/p^n}(m))) > \frac{1}{p^n}. \quad (12)$$

*Proof.* From the proof of Proposition 3.12,  $F'_n(\mathfrak{B}_{1/p^n}(m)) = F_n(\mathfrak{B}_{1/p^n}(m))$  for all  $m$ . The images coincide, so their diameters are equal and the classification is preserved.  $\square$

**Explicit Construction of Approximations.** The existence of  $n$ -th approximations is guaranteed by Theorem 3.9 (from  $\varepsilon$ -approximation theory in [28]). The explicit construction of some  $n$ -th approximations runs as follows. Let  $0 \leq n \leq N$ . The construction proceeds in several steps:

First, for each  $m = 0, 1, \dots, p^n - 1$ , we choose an auxiliary rational function  $g_m$  such that

$$g_m(\mathfrak{B}_{1/p^n}(m)) = \mathfrak{B}_{t_{n,m}}(\phi(m)). \quad (13)$$

A simple and computationally efficient choice is the affine function:

$$g_m(z) = A_m(z - m) + \beta_m, \quad (14)$$

where:

- $\beta_m = \phi(m) \bmod p^M$ , with  $M \in \mathbb{N}$  chosen so that  $t_{n,m} = 1/p^M$ ;
- $A_m \in \mathbb{C}_p$  is chosen to satisfy  $|A_m|_p = t_{n,m} \cdot p^n$ .

Coefficients lie in  $\mathbb{C}_p$ ; integrality (e.g. in  $\mathbb{Z}_p$ ) is not required for the construction. The existence of such  $A_m$  is guaranteed by standard arguments in ultrametric analysis (see [28, Section 3] for the explicit construction).

Second, to combine the local functions  $g_m$  into a global rational function, we use “gluing” functions  $h_m$  that act as a non-Archimedean partition of unity. As detailed in [28], we can take:

$$h_m(z) = \frac{1}{1 - \left(\frac{z-m}{c_m}\right)^{M_m}} \quad (15)$$

for appropriate choices of  $c_m \in \mathbb{C}_p$  and  $M_m \in \mathbb{N}$ .

**Remark 3.14** (Properties of the gluing functions [28]). *Let  $h_m$  be defined as in equation (15). For a suitable choice of  $c_m \in \mathbb{C}_p$  and  $M_m \in \mathbb{N}$  (see [28]), the following hold:*

- (i)  $h_m(z) = 1$  for all  $z \in B_{1/p^n}(m)$  (local selection property).
- (ii)  $|h_m(z)|_p < 1$  for all  $z \notin B_{1/p^n}(m)$  (decay outside the ball).
- (iii) The function  $h_m$  is well-defined and continuous on  $\mathbb{C}_p \setminus \{z : |z - m|_p = |c_m|_p\}$ , with its poles on the set  $\{z : |z - m|_p = |c_m|_p\}$  (the “metric boundary” of the ball, i.e. points at distance exactly  $|c_m|_p$  from  $m$ ; not a topological boundary; cf. Section 2).

*Proof.* Part (i): [28, Remark 4.3] gives the choice of  $M_m$  so that  $h_m(z) = 1$  on  $B_{1/p^n}(m)$ . Parts (ii) and (iii): [28, Section 4].  $\square$

Third, using Theorem 3.9 (which relies on Theorem 2.8 from [28]), we define the  $n$ -th approximation as:

$$F_n(z) = \sum_{m=0}^{p^n-1} g_m(z) \cdot h_m(z). \quad (16)$$

This construction ensures that  $F_n(\mathfrak{B}_{1/p^n}(m)) = \mathfrak{B}_{t_{n,m}}(\phi(m))$  for each  $m \in \{0, 1, \dots, p^n - 1\}$ , as required by the definition of  $n$ -th approximation.

**Remark 3.15** (Parameter choices and non-uniqueness of the approximation sequence). *For the canonical partition of  $\mathbb{Z}_p$  at radius  $1/p^n$ , the minimum inter-center distance is uniform:  $\delta = 1/p^{n-1}$ , so valid uniform parameters for (15) are  $|c_m|_p = p^{1/2}/p^n$  and  $M_m = 2N + 1$  (Remark 3.14). The choice of these parameters does not affect the mapping properties or the stability classification defined in Section 5. More generally, the choice of  $g_m$  and  $h_m$  affects the explicit form of  $F_n$  but not the mapping properties or the stability analysis; affine  $g_m(z) = A_m(z - m) + \beta_m$  are preferred for computational efficiency. The sequence  $\{F_n\}$  approximates some interpreter  $\phi$  (Proposition 3.11); extension beyond rational dynamics [5] is left for future work.*

**Classification of Ball-Level Dynamics.** To describe the behavior of  $f$  under the  $n$ -th approximation, we use the following definition.

**Definition 3.16.** *Let  $f : C \rightarrow C$  be a dynamical system with affinoid domain  $\mathcal{U} = \bigcup_{a \in C} \mathfrak{B}(a)$ , and let  $t_{n,m}$  be as in equation (5). For  $m \in \{0, \dots, p^n - 1\}$ , we say that the dynamics of  $f$  in  $\mathfrak{B}_{1/p^n}(m)$  is*

- $n$ -contracting if  $t_{n,m} < 1/p^n$ ;
- $n$ -expanding if  $t_{n,m} > 1/p^n$ ;
- $n$ -isometric if  $t_{n,m} = 1/p^n$ .

*When an  $n$ -approximation  $F_n$  exists and the image ball lies in the same ball chain as  $\mathfrak{B}_{1/p^n}(m)$ , this coincides with the set-inclusion formulation:  $F_n(\mathfrak{B}_{1/p^n}(m)) \subsetneq \mathfrak{B}_{1/p^n}(m)$  for contracting,  $\supsetneq$  for expanding, and  $=$  for isometric.*

Writing  $\Lambda_{n,m} := p^n t_{n,m}$  (the *coarse multiplier*; Section 5), the classification becomes  $\Lambda_{n,m} < 1$  (contracting),  $\Lambda_{n,m} > 1$  (expanding),  $\Lambda_{n,m} = 1$  (isometric), in direct analogy with the classical multiplier criterion  $|\phi'(x_0)|_p \leq 1$ . Theorem 5.5 implies that this classification is invariant under the choice of interpreter  $\phi$ .

**Remark 3.17** (Ball-level dynamics, fixed points, and terminology). *The classifications in Definition 3.16 connect directly to p-adic dynamics. By the ultrametric property, if the image ball  $F_n(\mathfrak{B}_{1/p^n}(m))$  intersects the domain ball  $\mathfrak{B}_{1/p^n}(m)$ , one contains the other (or they coincide). Since the construction of  $F_n$  as a gluing of rational functions places its poles outside  $\mathfrak{B}_{1/p^n}(m)$  [28],  $F_n$  is continuous on the ball; thus:*

- Contracting ( $t_{n,m} < 1/p^n$ ):  $F_n(\mathfrak{B}_{1/p^n}(m)) \subsetneq \mathfrak{B}_{1/p^n}(m)$ ; by [5, Theorem 4.7],  $F_n$  has a unique attracting fixed point in  $\mathfrak{B}_{1/p^n}(m)$ .
- Expanding ( $t_{n,m} > 1/p^n$ ):  $F_n(\mathfrak{B}_{1/p^n}(m)) \supsetneq \mathfrak{B}_{1/p^n}(m)$ ; if  $F_n$  is one-to-one on the ball (Proposition 2.7 (b)), there is a unique repelling fixed point. The approximation can be constructed to be one-to-one on each ball [28].
- Isometric ( $t_{n,m} = 1/p^n$ ):  $F_n(\mathfrak{B}_{1/p^n}(m)) = \mathfrak{B}_{1/p^n}(m)$ ; if moreover  $F_n$  is one-to-one on the ball (achievable by construction [28]), then  $F_n$  is bijective on the ball and any fixed points are indifferent (Proposition 2.7 (c)); existence is not guaranteed in this case.

When the image ball does not intersect the domain ball, no fixed point of  $F_n$  lies in the ball, regardless of the classification.

Several caveats apply. (i) Any fixed point of  $F_n$  guaranteed above lies in  $\mathbb{C}_p$ ; it need not belong to  $\mathbb{Z}_p$ , since  $\phi$  has coefficients in  $\mathbb{C}_p$  and the restriction of  $F_n$  to  $\mathbb{Z}_p$  need not map p-adic integer balls into themselves. Our ball-level classification is formulated on observable balls  $\mathfrak{B}_{1/p^n}(m) \cap \mathbb{Z}_p$  associated to discrete configurations; the full dynamics of  $F_n$  on  $\mathbb{C}_p$  may be more complex. (ii) The prefix “n-” reflects a ball-level property of  $F_n$  on  $\mathbb{C}_p$ -balls, not pointwise dynamics within  $\mathbb{Z}_p$ . (iii) The classification “n-expanding” indicates that the observable radius of the image is strictly larger than  $1/p^n$ ; it does not guarantee a classical repelling fixed point in the sense of  $|\phi'(x)|_p > 1$ . (iv) The classification depends on the gene ordering (Remark 3.18) and on the resolution level  $n$ . Throughout, we distinguish between fixed points in the combinatorial sense ( $f(a) = a$ ) and their ball-level classification as contracting or expanding, which depends on the p-adic ball and the resolution level, reflecting the hierarchical nature of the framework.

**Terminological convention.** In the application sections (Sections 6–7), we call a discrete fixed point of  $f$  attracting (resp. repelling) when it lies in an n-contracting (resp. n-expanding) ball whose image intersects the domain ball. Strictly, the fixed point of  $F_n$  is a point of  $\mathbb{C}_p$  that need not coincide with any configuration in  $\mathbb{Z}_p$ ; the discrete configurations in the ball inherit the classification by proximity. This is a deliberate abuse of notation; the precise ball-level formulation is in Definition 3.16.

**Remark 3.18** (Scope and dependence on gene ordering). *The analysis is constrained to the behavior of the approximations  $F_n$  on  $\mathbb{Z}_p$ ; no analytic continuation outside the ring of p-adic integers is assumed. Stability and optimal-order conclusions are stated for a fixed resolution  $N$  and fixed discrete dynamics  $f$ ; in this regime the partition and the measure  $\mu$  are well-defined and robust to the choice of approximants  $F_n$  (Section 5).*

All derived quantities depend on the gene ordering  $x_0, x_1, \dots, x_{N-1}$ ; this is a fundamental feature of the framework, not a limitation. Changing the order alters the embedding into  $\mathbb{Z}_p$ ; genes at lower powers of  $p$  have more influence on p-adic distances and hence on the ball-level classification. Different orderings produce different sequences  $F_0, \dots, F_N$  and may yield different classifications. Section 5 introduces a stability measure  $\mu$  that quantifies this dependence and identifies optimal orderings.

## 4. Illustrative Example: A Toy Model

We illustrate the framework with  $p = 2$ ,  $N = 4$ : we construct  $F_0, F_1, F_2, F_3$  explicitly and show how hierarchical analysis reveals stability structure.

Take  $p = 2$ ,  $N = 4$  (genes  $x_0, x_1, x_2, x_3$ );  $C$  has 16 elements. Configurations  $(a_0, a_1, a_2, a_3)$  correspond to  $m = a_0 + 2a_1 + 4a_2 + 8a_3 \in \{0, \dots, 15\}$ . The dynamics  $f$  is given by Table 2.

Let  $\phi \in \mathbb{C}_2(z)$  interpret  $f$  (Definition 3.1); then  $\phi(\mathfrak{B}(a)) \subseteq \mathfrak{B}(f(a))$ , and in our construction equality holds. Example:  $a = (0, 1, 0, 1)$  gives  $m = 10$ ,  $\mathfrak{B}(a) = \mathfrak{B}_{1/16}(10)$ ;  $f(a) = (0, 0, 1, 0)$  gives  $m' = 4$ , so  $\phi(\mathfrak{B}_{1/16}(10)) = \mathfrak{B}_{1/16}(4)$ .

**Construction of Hierarchical Approximations.** We compute  $F_0, F_1, F_2, F_3$  following Section 3. Throughout this subsection, we abbreviate  $\mathfrak{B}_{n,m} := \mathfrak{B}_{1/p^n}(m)$  for the closed ball in  $\mathbb{C}_p$  at level  $n$  with index  $m$ .

Config $(x_0, x_1, x_2, x_3)$	$m$	$f(x_0, x_1, x_2, x_3)$	$m'$
(0, 0, 0, 0)	0	(0, 0, 0, 0)	0
(1, 0, 0, 0)	1	(1, 0, 0, 0)	1
(0, 1, 0, 0)	2	(0, 0, 1, 0)	4
(1, 1, 0, 0)	3	(1, 0, 0, 1)	9
(0, 0, 1, 0)	4	(0, 0, 0, 0)	0
(1, 0, 1, 0)	5	(1, 0, 0, 1)	9
(0, 1, 1, 0)	6	(0, 0, 1, 0)	4
(1, 1, 1, 0)	7	(1, 0, 0, 0)	1
(0, 0, 0, 1)	8	(0, 0, 0, 0)	0
(1, 0, 0, 1)	9	(1, 0, 0, 0)	1
(0, 1, 0, 1)	10	(0, 0, 1, 0)	4
(1, 1, 0, 1)	11	(1, 0, 0, 1)	9
(0, 0, 1, 1)	12	(0, 0, 0, 0)	0
(1, 0, 1, 1)	13	(1, 0, 0, 1)	9
(0, 1, 1, 1)	14	(0, 0, 1, 0)	4
(1, 1, 1, 1)	15	(1, 0, 0, 0)	1

Table 2: Transition table for the toy example with  $N = 4$  genes. Each configuration  $(x_0, x_1, x_2, x_3)$  maps to its image under  $f$ . The integer representation  $m$  is computed as  $m = x_0 + 2x_1 + 4x_2 + 8x_3$ .

*Construction of  $F_0$ .* Every configuration  $a \in C$  satisfies  $\mathfrak{B}(a) \subset \mathfrak{B}_1(0)$ , so all 16 configurations lie in a single ball at level 0. The diameter of  $\phi(\mathfrak{B}_1(0))$  is

$$t_{0,0} = \max\{|\phi(x) - \phi(y)|_2 : x, y \in B_{0,0}\} = 1, \quad (17)$$

with center  $\beta_0 = 0$ . The required condition  $F_0(\mathfrak{B}_1(0)) = \mathfrak{B}_1(0)$  is met by choosing:

$$F_0(z) = z. \quad (18)$$

The coarsest level treats  $C$  as one ball; refinement at finer levels adds structure.

*Construction of  $F_1$ .* Recall that  $\mathfrak{B}_{1,0} = \mathfrak{B}_{1/2}(0)$  and  $\mathfrak{B}_{1,1} = \mathfrak{B}_{1/2}(1)$ .

If  $a, b \in C$  with  $\mathfrak{B}(a) \subset \mathfrak{B}_{1,0}$  and  $f(a) = b$ , then  $a = (0, a_1, a_2, a_3)$  for some  $a_1, a_2, a_3 \in \{0, 1\}$ ; that is, the configuration has first digit 0, so the corresponding integer  $m$  is in  $\{0, 2, 4, 6, 8, 10, 12, 14\}$ .

Examining the transition table, the images of these configurations are  $(0, 0, 0, 0)$  and  $(0, 0, 1, 0)$ , corresponding to integers 0 and 4 only. The 2-adic distance between these two images is  $|0 - 4|_2 = 1/4$ . Therefore, all images of configurations in  $\mathfrak{B}_{1,0}$  lie within a ball of radius  $1/4$ , and we can take  $\mathfrak{B}_{1/4}(0)$  as the containing ball. Hence,  $t_{1,0} = 1/4$ .

For the odd ball  $\mathfrak{B}_{1,1}$ : any  $a$  with  $\mathfrak{B}(a) \subset \mathfrak{B}_{1,1}$  has first digit 1, and the transition table shows every image satisfies  $b = (1, 0, 0, b_1)$  for some  $b_1 \in \{0, 1\}$ ; thus  $\mathfrak{B}(b) \subset \mathfrak{B}_{1/8}(1)$ , giving  $t_{1,1} = \frac{1}{8}$ ,  $\beta_1 = 1$ .

The 1-approximation is a rational function  $F_1 \in \mathbb{C}_2(z)$  such that  $F_1(\mathfrak{B}_{1/2}(0)) = \mathfrak{B}_{\frac{1}{4}}(0)$  and  $F_1(\mathfrak{B}_{1/2}(1)) = \mathfrak{B}_{\frac{1}{8}}(1)$ .

In this case, we can construct a 1-approximation  $F_1$  using the auxiliary functions:

$$g_0(z) = 2z \quad \text{and} \quad g_1(z) = 4(z - 1) + 1. \quad (19)$$

Then using the gluing technique from [28] we construct:

$$F_1(z) = \frac{2z}{1 - \left(\frac{z}{c_0}\right)^{M_0}} + \frac{4(z - 1) + 1}{1 - \left(\frac{z-1}{c_1}\right)^{M_1}}, \quad (20)$$

for some  $c_0, c_1 \in \mathbb{C}_2$  and  $M_0, M_1 \in \mathbb{N}$  chosen appropriately.

Since  $F_1(\mathfrak{B}_{1/2}(0)) = \mathfrak{B}_{\frac{1}{4}}(0) \subsetneq \mathfrak{B}_{1/2}(0)$ , the dynamics of  $f$  is 1-contracting in  $\mathfrak{B}_{1/2}(0)$ . By Remark 3.17, the rational function  $F_1$  has an attracting fixed point in  $\mathfrak{B}_{\frac{1}{4}}(0)$ .

On the other hand, since  $F_1(\mathfrak{B}_{1/2}(1)) = \mathfrak{B}_{\frac{1}{8}}(1) \subsetneq \mathfrak{B}_{1/2}(1)$ , the dynamics of  $f$  is 1-contracting in  $\mathfrak{B}_{1/2}(1)$ , and the rational function  $F_1$  has an attracting fixed point in  $\mathfrak{B}_{\frac{1}{8}}(1)$ .

Both level-1 balls are contracting; stable configurations appear at this scale.

*Construction of  $F_2$ .* At level 2,  $\mathfrak{B}_{2,m} = \mathfrak{B}_{1/4}(m)$  for  $m = 0, 1, 2, 3$ . Reading off the transition table gives  $t_{2,0} = t_{2,2} = \frac{1}{16}$ ,  $t_{2,1} = t_{2,3} = \frac{1}{8}$ ,  $\beta_0 = 0$ ,  $\beta_1 = \beta_3 = 1$ ,  $\beta_2 = 4$ ; a 2-approximation  $F_2 \in \mathbb{C}_2(z)$  must therefore satisfy:

$$\begin{aligned} F_2(\mathfrak{B}_{2,0}) &= \mathfrak{B}_{\frac{1}{16}}(0), & F_2(\mathfrak{B}_{2,1}) &= \mathfrak{B}_{\frac{1}{8}}(1), \\ F_2(\mathfrak{B}_{2,2}) &= \mathfrak{B}_{\frac{1}{16}}(4), & F_2(\mathfrak{B}_{2,3}) &= \mathfrak{B}_{\frac{1}{8}}(1). \end{aligned} \quad (21)$$

All the level-2 balls are contracting, however not all of them have an attracting fixed point, only the balls in which the image ball is contained in itself, as  $\mathfrak{B}_{2,0}$  and  $\mathfrak{B}_{2,1}$ .

*Construction of  $F_3$ .* Here the finest approximation is  $F_3$  (level  $n = 3$ ); for general  $N$ , the finest level is  $n = N$  and the corresponding approximation is  $F_N$ . At level 3,  $\mathfrak{B}_{3,m} = \mathfrak{B}_{1/8}(m)$  for  $m = 0, \dots, 7$ . The transition table yields  $t_{3,i} = \frac{1}{16}$  for all  $i$ , with centers  $\beta_0 = \beta_4 = 0$ ,  $\beta_1 = \beta_7 = 1$ ,  $\beta_2 = \beta_6 = 4$ ,  $\beta_3 = \beta_5 = 9$ ; the required ball maps are:

$$\begin{aligned} F_3(\mathfrak{B}_{3,0}) &= \mathfrak{B}_{\frac{1}{16}}(0), & F_3(\mathfrak{B}_{3,1}) &= \mathfrak{B}_{\frac{1}{16}}(1), \\ F_3(\mathfrak{B}_{3,2}) &= \mathfrak{B}_{\frac{1}{16}}(4), & F_3(\mathfrak{B}_{3,3}) &= \mathfrak{B}_{\frac{1}{16}}(9), \\ F_3(\mathfrak{B}_{3,4}) &= \mathfrak{B}_{\frac{1}{16}}(0), & F_3(\mathfrak{B}_{3,5}) &= \mathfrak{B}_{\frac{1}{16}}(9), \\ F_3(\mathfrak{B}_{3,6}) &= \mathfrak{B}_{\frac{1}{16}}(4), & F_3(\mathfrak{B}_{3,7}) &= \mathfrak{B}_{\frac{1}{16}}(1). \end{aligned} \quad (22)$$

Since  $t_{3,i} = \frac{1}{16} < \frac{1}{8}$  for every  $i$ , all eight balls are 3-contracting;  $F_3$  has attracting fixed points in  $\mathfrak{B}_{1/16}(0)$  and  $\mathfrak{B}_{1/16}(1)$ . These correspond to the two attracting fixed points  $(0, 0, 0, 0)$  and  $(1, 0, 0, 0)$  of  $f$  (Table 2). The example is modeled on  $z^2 \in \mathbb{C}_2(z)$ —whose attracting fixed points in  $\mathfrak{B}_1(0)$  are 0 and 1—and demonstrates that the hierarchical approximation recovers continuous dynamics from finite data. All quantities derive from  $f$  alone (Remark 3.5).

## 5. Stability Measure and Optimal Ordering

The gene ordering fixes the partition and hence the stability classification (Remark 3.18). This section defines a *stability measure*  $\mu$  on orderings: it quantifies, in a precise sense, how much expanding behavior appears across scales. Orderings that minimize  $\mu$  then correspond to the most stable hierarchical organization.

*Motivation.* If the network is organized hierarchically so that coarse-scale dynamics are stable, then a suitable ordering should yield few expanding balls.  $\mu$  makes this idea quantitative; minimizing  $\mu$  singles out orderings that expose that latent hierarchy.

*Encoding convention and canonical definitions.* All quantities below depend only on  $(f, \iota)$ . We fix the following convention.

**Remark 5.1** (Convention: encoding induced by the gene ordering). *Fix a bijection (encoding)*

$$\iota: C \longrightarrow \{0, 1, \dots, p^N - 1\}.$$

For  $n \leq N$ , the  $n$ -digit truncation is the map  $\text{trunc}_n: C \rightarrow \{0, \dots, p^n - 1\}$  given by  $\text{trunc}_n(a) := \iota(a) \bmod p^n$ . We write  $a \equiv b \pmod{p^n}$  if and only if  $\text{trunc}_n(a) = \text{trunc}_n(b)$ . The ball  $\mathfrak{B}_{1/p^n}(m)$  is the set of configurations with  $\text{trunc}_n(x) = m$  (same first  $n$  digits under  $\iota$ ). The index  $m \in \{0, \dots, p^n - 1\}$  of the ball  $\mathfrak{B}_{1/p^n}(m)$  corresponds to  $\text{trunc}_n(a) = m$ .

For  $n \in \{1, \dots, N - 1\}$ ,  $m \in \{0, \dots, p^n - 1\}$ , and  $k \in \{0, 1, \dots, N\}$ , define the set of image truncations at level  $k$  in the block indexed by  $m$ :

$$\mathcal{S}_n^{(k)}(m) := \{\iota(f(a)) \bmod p^k : a \in C, \text{trunc}_n(a) = m\} \subseteq \{0, \dots, p^k - 1\}.$$

The *maximum common prefix length* is

$$M_{n,m} := \max\{k \in \{0, \dots, N\} : |S_n^{(k)}(m)| = 1\}.$$

Since  $a \bmod 1 = 0$  for every integer  $a$ , we have  $|S_n^{(0)}(m)| = 1$  for all  $n, m$ , ensuring  $M_{n,m} \geq 0$ . Hence  $M_{n,m} \in \{0, \dots, N\}$ . The *observable radius*  $t_{n,m}$  (equation (5)) satisfies

$$t_{n,m} = \frac{1}{p^{M_{n,m}}},$$

providing a combinatorial interpretation:  $M_{n,m}$  is the number of shared leading  $p$ -adic digits among the images  $f(a)$  with  $a$  in the ball  $B_{1/p^n}(m)$ ; the larger  $M_{n,m}$ , the more concentrated the image in a small ball. The coarse multiplier (Section 3) satisfies

$$\Lambda_{n,m} = p^n t_{n,m} = p^{n-M_{n,m}}.$$

At level  $n$ , the domain ball has radius  $1/p^n$  and the image under an  $n$ -th approximation has radius  $t_{n,m} = 1/p^{M_{n,m}}$ ; the ratio  $\Lambda_{n,m} = t_{n,m}/(1/p^n) = p^{n-M_{n,m}}$  is the expansion factor and plays the role of the classical multiplier  $|\phi'(x_0)|_p$  in dynamics (cf. [5, Proposition 3.20]). An  $n$ -th approximation is any rational function  $F_n$  satisfying Definition 3.8 (as provided by the  $\varepsilon$ -approximation framework of [28]); for such  $F_n$ , this ratio coincides with  $|F'_n|_p$  at some point of the ball (see [5, Proposition 3.20]). Any two such approximations are uniformly close on each  $B_{n,m}$  (Proposition 3.12), so  $\Lambda_{n,m}$  and the stability classification do not depend on the choice of  $F_n$ . One may *choose* an  $n$ -th approximation that is piecewise affine on the partition (e.g. the explicit construction in Section 3, equation (14)); in that case  $|F'_n|_p$  is constant on each  $B_{n,m}$  and the equality  $|F'_n(z)|_p = \Lambda_{n,m}$  holds exactly for all  $z$  in the ball. In terms of  $M_{n,m}$ :  $M_{n,m} < n \Leftrightarrow$  expanding,  $M_{n,m} = n \Leftrightarrow$  isometric,  $M_{n,m} > n \Leftrightarrow$  contracting. The counts per level are

$$E(n) := \#\{m : M_{n,m} < n\}, \quad I(n) := \#\{m : M_{n,m} = n\}, \quad A(n) := \#\{m : M_{n,m} > n\},$$

so that  $E(n) + I(n) + A(n) = p^n$ . The three stability scores are

$$\begin{aligned} \mu_E &:= \sum_{n=1}^{N-1} E(n) \cdot p^{N-n}, \\ \mu_A &:= \sum_{n=1}^{N-1} A(n) \cdot p^{N-n}, \\ \mu_I &:= \sum_{n=1}^{N-1} I(n) \cdot p^{N-n}. \end{aligned}$$

**Lemma 5.2** (Control identity).  $\mu_E + \mu_A + \mu_I = (N-1)p^N$ .

*Proof.*  $E(n) + I(n) + A(n) = p^n$  implies  $\sum_{n=1}^{N-1} (E(n) + A(n) + I(n)) p^{N-n} = \sum_{n=1}^{N-1} p^N = (N-1)p^N$ .  $\square$

**Remark 5.3** (Multi-objective trade-off). Since  $\mu_E + \mu_A + \mu_I$  is constant, minimizing  $\mu_E$  is equivalent to maximizing  $\mu_A + \mu_I$ , not to maximizing  $\mu_A$  alone. In particular, the set of orderings that minimize  $\mu_E$  and the set that maximize  $\mu_A$  can be—and in general are—disjoint. Part II [30] confirms this empirically for the *A. thaliana* network and explores the resulting trade-off.

**Definition of Stability Measure.** We define the stability measure  $\mu$  and the set of expanding balls from the canonical quantities above.

**Definition 5.4.** Let  $(x_{\alpha_0}, \dots, x_{\alpha_{N-1}})$  be an ordering of the  $N$  genes in the GRN and let  $t, M_{n,m}, t_{n,m}$  be as in Section 5. For each resolution level  $n$  with  $1 \leq n \leq N-1$ , the set of expanding balls at level  $n$  is

$$C(n) = \{m \in \{0, 1, \dots, p^n - 1\} : M_{n,m} < n\} = \{m : t_{n,m} > 1/p^n\}. \quad (23)$$

The stability measure  $\mu$  of the ordering is

$$\mu(x_{\alpha_0}, \dots, x_{\alpha_{N-1}}) = \sum_{n=1}^{N-1} |C(n)| \cdot p^{N-n} = \mu_E. \quad (24)$$

By Corollary 3.13,  $\mu$  is also invariant under perturbations of the approximations  $F_n$  satisfying the bound in Proposition 3.12. When an interpreter  $\phi$  and approximants  $F_n$  exist,  $t_{n,m}$  coincides with  $\text{rad}_{\mathbb{Z}_p}(F_n(B_{n,m}))$  (Definition 5.6 below), so  $C(n) = \{m : \text{diam}(F_n(B_{1/p^n}(m))) > 1/p^n\}$ ; the discrete definition ensures  $\mu_E, \mu_A, \mu_I$  depend only on  $(f, \iota)$ . Smaller  $\mu$  corresponds to fewer expanding balls across scales; the weights guarantee that coarser-scale instabilities count more than finer ones.

**Theorem 5.5** (Intrinsic nature of  $\mu_*$ ). *The quantities  $t_{n,m}, \Lambda_{n,m}$ , the counts  $E(n), A(n), I(n)$ , and the scores  $\mu_E, \mu_A, \mu_I$  depend only on  $(f, \iota)$  and are independent of any interpreter  $\phi$  and of the approximants  $F_n$ .*

*Proof.* All are defined explicitly from  $f$  and  $\text{trunc}_n$  (Convention 5.1 and the definitions in Section 5). In particular,  $t_{n,m} = 1/p^{M_{n,m}}$  coincides with the  $\phi$ -based radius in equation (5) (Remark 3.5), so the stability invariants can be evaluated from  $(f, \iota)$  without constructing  $\phi$  explicitly <sup>1</sup>.  $\square$

Theorem 5.5 is a *computability result*: the stability invariants, originally defined through the dynamics of rational functions over  $\mathbb{C}_p$ , turn out to be evaluable from the discrete data  $(f, \iota)$ . The theory of non-Archimedean dynamics over  $\mathbb{C}_p$  is not an auxiliary convenience but a mathematical necessity; three ingredients of the framework require  $\mathbb{C}_p$  specifically:

- (i) *Existence of interpreters and approximations* (Corollary 3.3, Theorem 3.9). The  $\varepsilon$ -approximation technique of [28] builds global rational functions from local data on disjoint balls; the gluing functions  $h_m$  (equation (15)) require parameters  $c_m$  whose  $p$ -adic valuation is non-integral ( $|c_m|_p = p^{1/2}/p^n$ ; Remark 3.15). No element of  $\mathbb{Q}_p$  has half-integral valuation (the value group of  $\mathbb{Q}_p$  is  $p^{\mathbb{Z}}$ ), so these coefficients exist in  $\mathbb{C}_p$  but not in  $\mathbb{Q}_p$ .
- (ii) *Fixed-point theory* (Proposition 2.7). The existence of a unique attracting (resp. repelling) fixed point in a contracting (resp. expanding) ball is a theorem in  $\mathbb{C}_p$  dynamics [5, Thm. 4.18]; the fixed point lives in  $\mathbb{C}_p$  and need not belong to  $\mathbb{Z}_p$ . This is what gives the contracting/expanding/isometric classification its dynamical content: it extends the attracting/repelling/indifferent trichotomy of Proposition 2.7 from individual fixed points to entire balls.

The observable radius  $t_{n,m}$  coincides with the image radius under an  $n$ -th approximation  $F_n$  (Definition (3.8)); the coarse multiplier  $\Lambda_{n,m}$  is the ball-level analogue of the classical multiplier  $|F'_n(x_0)|_p$ ; and the classification (Definition 3.16) extends the classical trichotomy to ball-level dynamics. Without  $\mathbb{C}_p$ , one could still define  $M_{n,m}$  as a combinatorial statistic (the maximum common prefix length of images), but there would be no mathematical reason to call  $M_{n,m} < n$  “expanding” or to connect it to repelling dynamics. The discrete formulae of Theorem 5.5 are therefore not *ad hoc* combinatorial definitions but the computable shadow of a richer analytical structure—one that also provides the natural setting for future extensions such as perturbation analysis of interpreters and connections to Berkovich analytic spaces (cf. footnote 1).

*Observable  $\mathbb{Z}_p$ -radius and integral formulation.* Let  $B_{n,m} = m + p^n\mathbb{Z}_p \subset \mathbb{Z}_p$  denote the ball at resolution  $p^{-n}$ . An interpreter and, for each  $n$ , an  $n$ -th approximation  $F_n$  exist (Corollary 3.3, Section 3). The canonical  $t_{n,m}$  therefore coincides with the following observable radius applied to the image  $F_n(B_{n,m})$ ; this quantity is used to express  $t_{n,m}$  as the radius of the image set and in the integral formulation (Remark 5.7).

**Definition 5.6** ( $\mathbb{Z}_p$ -observable radius). *Let  $U \subset \mathbb{C}_p$  with  $U \cap \mathbb{Z}_p \neq \emptyset$ . The  $\mathbb{Z}_p$ -observable radius of  $U$  is*

$$\text{rad}_{\mathbb{Z}_p}(U) := \inf \{r \geq 0 : \exists a \in \mathbb{Z}_p \text{ such that } U \cap \mathbb{Z}_p \subseteq B_r(a)\}.$$

*Equivalently,  $\text{rad}_{\mathbb{Z}_p}(U) = \sup\{|x - y|_p : x, y \in U \cap \mathbb{Z}_p\}$ . If  $U \cap \mathbb{Z}_p$  is a single point, then  $\text{rad}_{\mathbb{Z}_p}(U) = 0$ .*

Recall that the *normalized Haar measure* on  $\mathbb{Z}_p$  (see Section 2 and [41]) is the unique translation-invariant Borel probability measure on  $\mathbb{Z}_p$ ; we denote it by  $\lambda_H$  to avoid confusion with the stability measure  $\mu$ , and it satisfies  $\lambda_H(B_{1/p^n}(m)) = p^{-n}$  for each ball of the partition.

<sup>1</sup>Even though their definition and dynamical interpretation rest on the analytical framework in  $\mathbb{C}_p$  developed in Sections 2–3.

**Remark 5.7** (Haar integral formulation). Let  $\lambda_H$  denote the normalized Haar measure on  $\mathbb{Z}_p$  (so that  $\lambda_H(B_{1/p^n}(m)) = p^{-n}$ ). For  $x \in \mathbb{Z}_p$ , let  $m_n(x) \in \{0, \dots, p^n - 1\}$  be the index of the ball containing  $x$ . The indicators

$$\mathbf{1}_{E,n}(x) = \mathbf{1}_{\{\Lambda_{n,m_n(x)} > 1\}}, \quad \mathbf{1}_{A,n}(x) = \mathbf{1}_{\{\Lambda_{n,m_n(x)} < 1\}}, \quad \mathbf{1}_{I,n}(x) = \mathbf{1}_{\{\Lambda_{n,m_n(x)} = 1\}}$$

are locally constant on balls at level  $n$ . Then

$$\mu_* = p^N \sum_{n=1}^{N-1} \int_{\mathbb{Z}_p} \mathbf{1}_{*,n}(x) d\lambda_H(x), \quad * \in \{E, A, I\}.$$

*Proof.*  $\mathbf{1}_{*,n}$  is constant on each  $B_{1/p^n}(m)$ , so  $\int_{\mathbb{Z}_p} \mathbf{1}_{*,n} d\lambda_H$  equals the Haar measure of the set  $\{x : \Lambda_{n,m_n(x)} * 1\}$ , which is the count of balls of that type times  $p^{-n}$ . Multiplying by  $p^N$  and summing over  $n$  yields the weighted counts defining  $\mu_E, \mu_A, \mu_I$ .  $\square$

**Remark 5.8** (Interpretation of the weight and volume). The weight  $p^{N-n}$  in the definition of  $\mu$  has three complementary interpretations.

(i) Combinatorial. The space  $\mathcal{C}$  has  $p^N$  configurations. At level  $n$ ,  $\mathbb{Z}_p$  is partitioned into  $p^n$  balls  $B_{1/p^n}(m)$ , each containing exactly  $p^{N-n}$  configurations. Thus  $p^{N-n}$  is the number of configurations in each ball at that level. The sum  $\mu_E = \sum_{n=1}^{N-1} E(n) \cdot p^{N-n}$  is the total number of “configuration–level” contributions to expanding dynamics: each of the  $E(n)$  expanding balls at level  $n$  is weighted by the  $p^{N-n}$  configurations it contains. Coarser scales (small  $n$ ) contribute more because their balls have larger mass  $p^{N-n}$ .

(ii) Measure-theoretic. Let  $\lambda_H$  denote the normalized Haar measure on  $\mathbb{Z}_p$ , so  $\lambda_H(B_{n,m}) = p^{-n}$ . The set  $\{x \in \mathbb{Z}_p : \Lambda_{n,m_n(x)} > 1\}$  (expanding at level  $n$ ) has Haar measure  $E(n) \cdot p^{-n}$ . By definition,  $\mu_E = \sum_{n=1}^{N-1} E(n) \cdot p^{N-n}$  (equation (24)). Since  $p^{N-n} = p^N \cdot p^{-n}$ , this is the same as  $\mu_E = p^N \sum_{n=1}^{N-1} E(n) \cdot p^{-n}$ : a single factor  $p^N$  (the cardinality of  $\mathcal{C}$ ) multiplies the sum of the Haar proportions  $E(n)/p^n$ , so  $p^N$  converts those proportions into configuration counts. Equivalently,  $p^{N-n} = p^N \cdot \lambda_H(B_{n,m})$  is the number of configurations in  $B_{n,m}$ , so the weight multiplies the count  $E(n)$ , not the fraction  $E(n)/p^n$ .

(iii) Canonicity and alternatives. The Haar measure  $\lambda_H$  is the unique translation-invariant Borel probability measure on  $\mathbb{Z}_p$  [41], so the dependence on scale,  $\lambda_H(B_{n,m}) = p^{-n}$ , is fixed by the  $p$ -adic structure. The factor  $p^N$  is determined by the requirement that  $p^{N-n}$  equal the number of configurations in  $B_{n,m}$ ; no free parameter enters. The uniform weight  $\sum_n E(n)$  treats all balls equally and discards the hierarchy. The fractional weight  $\sum_n E(n)/p^n = \mu_E/p^N$  has the same minimizers as  $\mu_E$  (Proposition 5.7), which confirms internal consistency. Other weights (e.g. entropic) would require separate justification. The sum runs from  $n = 1$  to  $N - 1$ : at  $n = 0$  there is a single ball and at  $n = N$  each ball is a singleton, so neither yields hierarchical information.

*Properties of the Stability Measure.* The sum in (24) runs from  $n = 1$  to  $N - 1$ : at  $n = 0$  there is only one ball ( $\mathbb{Z}_p$  itself), so no hierarchical information is available; levels  $n = 1$  to  $N - 1$  capture the full stratification from coarsest to finest. The bounds  $0 \leq \mu \leq (N - 1)p^N$  are immediate from  $|C(n)| \in [0, p^n]$ ; the upper bound is achieved only when every ball is expanding at every level.

We adopt  $\mu_E$  as the primary optimization criterion throughout this paper. Expanding dynamics at coarse scales signals that configurations agreeing in the most influential genes—those occupying the leading  $p$ -adic positions—diverge under  $f$ ; this is a direct obstruction to hierarchical stability. By contrast, contraction at fine scales merely indicates local convergence among configurations that already differ in high-level regulators (Remark 5.8). Part II [30] examines the complementary criterion (maximizing  $\mu_A$ ); the trade-off is governed by Lemma 5.2.

Minimizing  $\mu$  has a natural evolutionary interpretation: perturbations to master regulators propagate to all downstream targets, while peripheral-gene noise has localized effects. Organisms that place high-influence genes such that coarse-scale dynamics are contracting tolerate stochastic fluctuations without catastrophic consequences—a selective advantage consistent with the observation that master regulators are typically more conserved across species than peripheral genes [1, 15].

**Definition 5.9.** Let  $(x_{\alpha_0}, \dots, x_{\alpha_{N-1}})$  and  $(x_{\beta_0}, \dots, x_{\beta_{N-1}})$  be two different orderings of the same  $N$  genes.

We say that the ordering  $(x_{\alpha_0}, \dots, x_{\alpha_{N-1}})$  is more stable than the ordering  $(x_{\beta_0}, \dots, x_{\beta_{N-1}})$  if:

$$\mu(x_{\alpha_0}, \dots, x_{\alpha_{N-1}}) < \mu(x_{\beta_0}, \dots, x_{\beta_{N-1}}). \quad (25)$$

The measure  $\mu$  induces a total preorder on the set of orderings. Different orderings give different  $|C(n)|$  at each level; the minimizers are those that concentrate stability at coarse scales. In applications, orderings that place master regulators early often achieve low  $\mu$ , consistent with their stabilizing role.

*Finding optimal orderings.* The mathematical problem is to minimize  $\mu$  over the  $N!$  orderings. For a given ordering,  $\mu$  is determined by  $(f, i)$  alone (Remark 3.5); no construction of  $F_n$  or  $\phi$  is required.

The cost of minimizing  $\mu$  for one ordering is  $O(N \cdot p^N)$ , which is feasible for  $N \leq 15$ . For small  $N$  (e.g.  $N \leq 8$ ) minimization over all  $N!$  orderings can be done by exhaustive enumeration. For  $N = 13$ , Part II [30] certifies the four  $\mu_E$ -minimizers by branch-and-bound over all  $13!$  orderings; in this paper, we also employ a genetic algorithm, both as independent verification and as a general-purpose method applicable to networks where branch-and-bound may not scale.

## 6. Application to *Arabidopsis thaliana*

The framework of Sections 3–5 is applied to the floral development network of *A. thaliana*. The section illustrates the mathematical theory on a well-studied Boolean model; the choice of network provides both a concrete illustration and a non-trivial validation of the mathematical framework.

The *A. thaliana* floral development network has a well-established Boolean model [18, 27] (cell fate, robustness, agreement with expression data), extended to the full flowering transition pathway in [12], and is a standard benchmark in GRN analysis [2]; we use it here to illustrate the measure  $\mu$ , the classification of fixed points, and the role of ordering. We adopt the standard ABC model nomenclature for organ identities (Sepal, Petal, Stamen, Carpel, Inflorescence) and gene names (AP1, AP2, AG, PI, AP3, etc.) as in [18, 27], consistently throughout. The optimal gene ordering is not assumed from experiment; it is derived by minimizing  $\mu$  from the dynamics  $f$  alone (the Boolean model does not prescribe an order—our framework selects it from the discrete map).

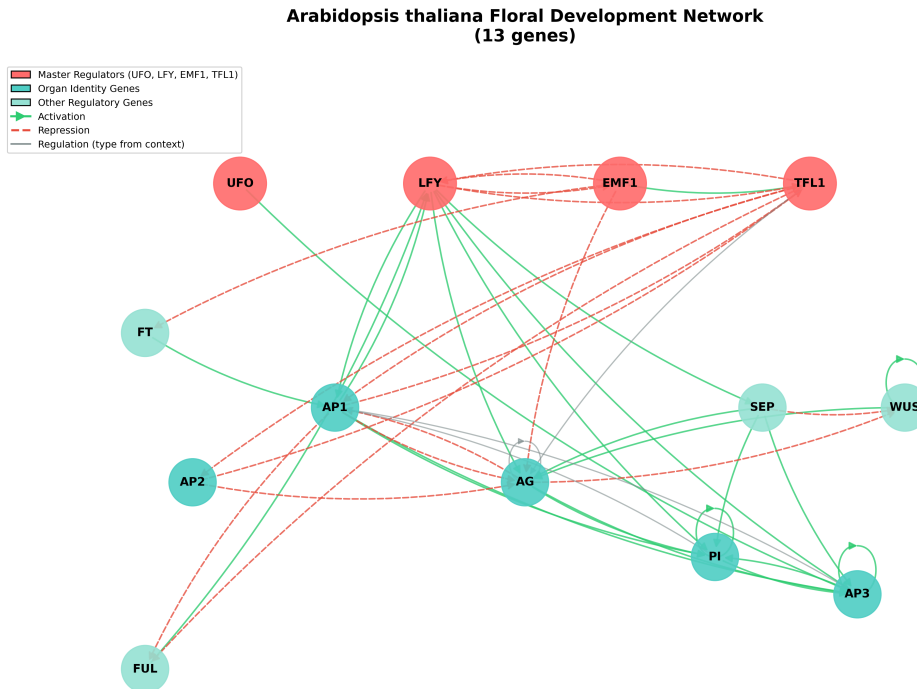


Figure 5: *A. thaliana* floral development network ( $N = 13$  genes). Node colors: red = top-ranked genes in  $\pi^*$  (UFO, EMF1, LFY, TFL1), dark teal = organ identity genes (AP1, AP2, AG, PI, AP3), light teal = other regulatory genes (FT, FUL, WUS, SEP). Edge styles: solid green arrows = activation, dashed red = repression, solid gray = regulation with context-dependent effect. Network topology and interaction types from [18, 27].

The regulatory network (Figure 5) and the transition table defining  $f$  are taken from [18, 27]. In those articles, the authors report the fixed points (attractors) of the network and identify each with a floral organ identity: inflorescence, sepal, petal, stamen, or carpel (the correspondence under our ordering  $\pi^*$  is given in Table 4). The gene order used in the reference to write the state vector is the *original-model ordering*; we compare it with the  $\mu$ -minimizing ordering in Section 7. The network has  $N = 13$  genes with states in  $\{0, 1\}$ , so  $C$  has  $2^{13}$  configurations; the map  $f : C \rightarrow C$  is given by synchronous update of that Boolean model. The object of interest is an ordering that minimizes  $\mu$ . For  $N = 13$ , the ordering used here is one of the four  $\mu_E$ -minimizers over all  $13!$  orderings, certified by branch-and-bound in Part II [30]; a genetic algorithm independently recovers the same optimum and serves as a general-purpose method for networks where exhaustive certification is infeasible. Denote this ordering by  $\pi^*$ :

$$\begin{aligned} & (x_0, x_1, x_2, x_3, x_4, x_5, x_6, x_7, x_8, x_9, x_{10}, x_{11}, x_{12}) \\ & \parallel \\ & (\text{UFO, EMF1, LFY, TFL1, AP2, FT, AG, AP1, SEP, AP3, PI, WUS, FUL}). \end{aligned} \quad (26)$$

Under  $\pi^*$ , configurations that differ only in later genes are close in the  $p$ -adic metric; those differing in early genes (UFO, EMF1, LFY, ...) are distant. The value  $\mu(\pi^*)$  is 26,776 (evaluated from  $f$  and  $t_{\pi^*}$  as in Section 5). All results in this section refer to this ordering. The first four positions are occupied by UFO, EMF1, LFY, and TFL1—the four top-ranked genes in Figure 5, identified as key regulators in [18, 27]—while downstream organ identity genes (AP2, FT, AG, AP1, ...) follow (Table 3). Four orderings attain  $\mu_E = 26,776$ ; they differ from  $\pi^*$  by transpositions in two pairs of positions (EMF1, LFY and AP2, FT) and share the same tail (genes in positions 7–13).

**Remark 6.1** (Symmetry of the  $\mu_E$ -optimal set). *Four orderings attain the minimum  $\mu_E = 26,776$ . They are obtained from  $\pi^*$  by swapping the genes in positions 2 and 3 (EMF1 and LFY) and/or the genes in positions 5 and 6 (AP2 and FT). Each such swap preserves  $(\mu_E, \mu_A, \mu_I)$  because these pairs play symmetric roles in the dynamics with respect to the leading-position structure; the group of such swaps has order 4, which accounts for exactly the four orderings observed. Exhaustive enumeration confirms that no other ordering attains  $\mu_E = 26,776$ . In biological terms, each pair (EMF1/LFY and AP2/FT) occupies the same hierarchical level for stability purposes: interchanging them does not alter the expanding, contracting, or isometric classification at any scale.*

Pos.	Gene	Biological Role	Key phenotype (refs.)
1	UFO	Organ identity modulator	Petal/stamen defects
2	EMF1	Flowering repressor	<i>emf1</i> : flower early
3	LFY	Master regulator, floral identity	<i>leafy</i> mutants fail to flower
4	TFL1	Inflorescence identity	<i>tfl1</i> : terminal flower
5	AP2	Organ identity, represses AG	Homeotic transformations
6	FT	Flowering promoter	Late flowering mutants
7	AG	Stamen/carpel identity	No reproductive organs
8	AP1	Floral meristem identity	Inflorescence-like structures

Table 3: Top eight positions in  $\pi^*$  (Eq. (26)) with their established biological roles and key mutant phenotypes. The first four positions coincide with the top-ranked genes of the *A. thaliana* floral GRN; the remaining positions contain organ identity and timing genes. Roles and phenotypes from [18, 27].

With this ordering, the partition at each scale and hence the stability classification are fixed (Remark 3.18); the leading positions are occupied by key regulators.

*Construction of Hierarchical Approximations.* The rational approximations  $F_0, \dots, F_4$  for this network encode the dynamics of  $f$  at each scale; their construction follows Section 3.

Throughout this subsection, balls are classified as contracting, expanding, or isometric according to the criterion of Section 5: a ball  $\mathfrak{B}_{1/p^n}(m)$  is contracting if  $M_{n,m} > n$  (equivalently,  $t_{n,m} < 1/p^n$ ), expanding if  $M_{n,m} < n$ , and isometric

if  $M_{n,m} = n$ . This criterion coincides with Definition 3.16 when the image ball lies within  $\mathfrak{B}_{1/p^n}(m)$  itself (contracting case) or contains it (expanding case).

Let  $\phi \in \mathbb{C}_2(z)$  be a rational function which interprets the dynamics of  $f$ . By definition of  $\phi$ , we need  $F_0(\mathfrak{B}_1(0)) = \mathfrak{B}_1(0)$ , so we can choose  $F_0(z) = z$ . For  $F_1$ , any 1-approximation  $F_1 \in \mathbb{C}_2(z)$  should satisfy:

$$\begin{aligned} F_1(\mathfrak{B}_{1/2}(0)) &= \mathfrak{B}_{1/2}(0), \\ F_1(\mathfrak{B}_{1/2}(1)) &= \mathfrak{B}_{1/2}(1). \end{aligned} \quad (27)$$

For example, we can take  $F_1(z) = z$ . Any 2-approximation  $F_2 \in \mathbb{C}_2(z)$  should satisfy:

$$\begin{aligned} F_2(\mathfrak{B}_{1/4}(0)) &= \mathfrak{B}_{1/2}(0), & F_2(\mathfrak{B}_{1/4}(1)) &= \mathfrak{B}_{1/2}(1), \\ F_2(\mathfrak{B}_{1/4}(2)) &= \mathfrak{B}_{1/2}(0), & F_2(\mathfrak{B}_{1/4}(3)) &= \mathfrak{B}_{1/2}(1). \end{aligned} \quad (28)$$

Using Theorem 3.9, we can construct the rational function  $F_2$  with the appropriate properties.

Since  $F_2(\mathfrak{B}_{1/4}(0)) = \mathfrak{B}_{1/2}(0) \supsetneq \mathfrak{B}_{1/4}(0)$ , the dynamics of  $f$  is 2-expanding in  $\mathfrak{B}_{1/4}(0)$ , and similarly in  $\mathfrak{B}_{1/4}(1)$ ,  $\mathfrak{B}_{1/4}(2)$  and  $\mathfrak{B}_{1/4}(3)$ . Any 3-approximation  $F_3 \in \mathbb{C}_2(z)$  should satisfy:

$$\begin{aligned} F_3(\mathfrak{B}_{1/8}(0)) &= \mathfrak{B}_{1/16}(6), & F_3(\mathfrak{B}_{1/8}(1)) &= \mathfrak{B}_{1/16}(7), \\ F_3(\mathfrak{B}_{1/8}(2)) &= \mathfrak{B}_{1/4}(2), & F_3(\mathfrak{B}_{1/8}(3)) &= \mathfrak{B}_{1/4}(3), \\ F_3(\mathfrak{B}_{1/8}(4)) &= \mathfrak{B}_{1/16}(4), & F_3(\mathfrak{B}_{1/8}(5)) &= \mathfrak{B}_{1/16}(5), \\ F_3(\mathfrak{B}_{1/8}(6)) &= \mathfrak{B}_{1/4}(0), & F_3(\mathfrak{B}_{1/8}(7)) &= \mathfrak{B}_{1/4}(1). \end{aligned} \quad (29)$$

The dynamics of  $f$  is 3-expanding in  $\mathfrak{B}_{1/8}(2)$ ,  $\mathfrak{B}_{1/8}(3)$ ,  $\mathfrak{B}_{1/8}(6)$  and  $\mathfrak{B}_{1/8}(7)$  (image radius  $1/4 > 1/8$ ), and 3-contracting in  $\mathfrak{B}_{1/8}(0)$ ,  $\mathfrak{B}_{1/8}(1)$ ,  $\mathfrak{B}_{1/8}(4)$  and  $\mathfrak{B}_{1/8}(5)$  (images  $\mathfrak{B}_{1/16}(6)$ ,  $\mathfrak{B}_{1/16}(7)$ ,  $\mathfrak{B}_{1/16}(4)$ ,  $\mathfrak{B}_{1/16}(5)$  respectively). Any 4-approximation  $F_4 \in \mathbb{C}_2(z)$  should satisfy:

$$\begin{aligned} F_4(\mathfrak{B}_{1/16}(0)) &= \mathfrak{B}_{1/64}(54), & F_4(\mathfrak{B}_{1/16}(1)) &= \mathfrak{B}_{1/64}(55), \\ F_4(\mathfrak{B}_{1/16}(2)) &= \mathfrak{B}_{1/8}(6), & F_4(\mathfrak{B}_{1/16}(3)) &= \mathfrak{B}_{1/8}(7), \\ F_4(\mathfrak{B}_{1/16}(4)) &= \mathfrak{B}_{1/64}(52), & F_4(\mathfrak{B}_{1/16}(5)) &= \mathfrak{B}_{1/64}(53), \\ F_4(\mathfrak{B}_{1/16}(6)) &= \mathfrak{B}_{1/128}(20), & F_4(\mathfrak{B}_{1/16}(7)) &= \mathfrak{B}_{1/128}(21), \\ F_4(\mathfrak{B}_{1/16}(8)) &= \mathfrak{B}_{1/128}(38), & F_4(\mathfrak{B}_{1/16}(9)) &= \mathfrak{B}_{1/128}(39), \\ F_4(\mathfrak{B}_{1/16}(10)) &= \mathfrak{B}_{1/8}(2), & F_4(\mathfrak{B}_{1/16}(11)) &= \mathfrak{B}_{1/8}(3), \\ F_4(\mathfrak{B}_{1/16}(12)) &= \mathfrak{B}_{1/64}(36), & F_4(\mathfrak{B}_{1/16}(13)) &= \mathfrak{B}_{1/64}(37), \\ F_4(\mathfrak{B}_{1/16}(14)) &= \mathfrak{B}_{1/128}(0), & F_4(\mathfrak{B}_{1/16}(15)) &= \mathfrak{B}_{1/128}(1). \end{aligned} \quad (30)$$

The dynamics of  $f$  is 4-contracting in  $\mathfrak{B}_{1/16}(4)$  and  $\mathfrak{B}_{1/16}(5)$ , and 4-expanding in  $\mathfrak{B}_{1/16}(10)$  and  $\mathfrak{B}_{1/16}(11)$ . The hierarchical refinement is visible across levels: at  $n = 3$ , expanding dynamics occupies  $\mathfrak{B}_{1/8}(2)$ ,  $\mathfrak{B}_{1/8}(3)$ ,  $\mathfrak{B}_{1/8}(6)$ ,  $\mathfrak{B}_{1/8}(7)$ ; at  $n = 4$ , it localizes to  $\mathfrak{B}_{1/16}(10)$  and  $\mathfrak{B}_{1/16}(11)$  (since  $\mathfrak{B}_{1/16}(10) \subsetneq \mathfrak{B}_{1/8}(2)$ ,  $\mathfrak{B}_{1/16}(11) \subsetneq \mathfrak{B}_{1/8}(3)$ ), progressively pinpointing the inflorescence configurations.

*Identification of Attractors and Repellers.* Mendoza and Espinosa-Soto et al. [18, 27] identify the fixed points of this network and their correspondence to floral organ identities (see also [29]). The terminological conventions for *fixed point*, *attracting*, and *repelling* follow Remark 3.17; the ball-level classification (Definition 3.16) gives a finer picture than treating all fixed points as equivalent attractors.

Under the ordering  $\pi^*$  (one of the four  $\mu_E$ -minimizers; Eq. (26), Table 3),  $f$  has exactly 10 fixed points, grouped in four balls at resolution  $n = 4$ . Configuration indices in this subsection and in Table 4 use the encoding  $m = \sum_{k=0}^{N-1} x_{\alpha_k} 2^k$  with  $\pi^*$ ; ball assignment depends on the chosen ordering.

The six organ-identity fixed points lie in two contracting balls:  $\mathfrak{B}_{1/16}(4)$  contains configurations 436, 1972, 5492, and 6004 (UFO=0, EMF1=0, LFY=1, TFL1=0; Sepal, Petal, Carpel, and Stamen in the ABC interpretation), and  $\mathfrak{B}_{1/16}(5)$  contains 1973 and 6005 (UFO=1, EMF1=0, LFY=1, TFL1=0; the UFO-active Petal and Stamen variants).

The four inflorescence fixed points distribute equally between two expanding balls:  $\mathfrak{B}_{1/16}(10)$  holds configurations 10 and 2058 (UFO=0, EMF1=1, LFY=0, TFL1=1), and  $\mathfrak{B}_{1/16}(11)$  holds 11 and 2059 (UFO=1, same inflorescence pattern); both balls exhibit expanding dynamics (Table 4).

So mature organs sit in contracting balls (stable endpoints) and inflorescence states in expanding balls (transient). The 10 fixed points and their organ identities match the ABC interpretation of [18, 27]: Sepal 436; Petal 1972, 1973; Stamen 6004, 6005; Carpel 5492; Inflorescence 10, 2058, 11, 2059 (LFY=0).

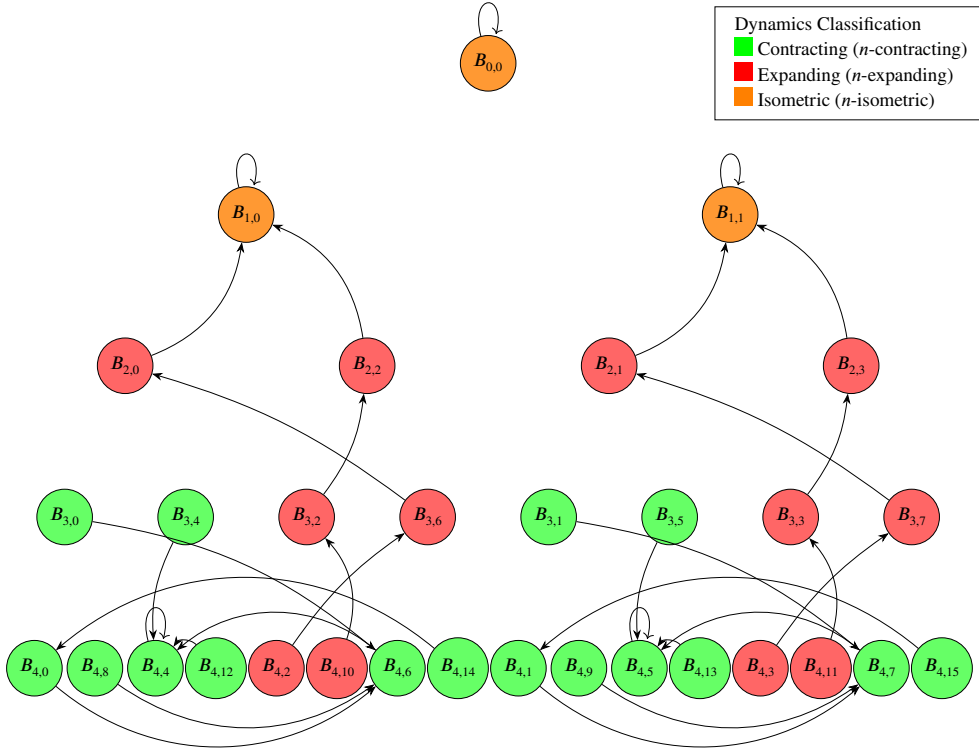


Figure 6:  $p$ -adic ball structure for *A. thaliana*, levels  $n = 0-4$ . Green: contracting; red: expanding; yellow: isometric. Ordering  $\pi^*$  (Eq. (26)), dynamics  $f$  from [18, 27].  $\mathfrak{B}_{1/16}(4)$  and  $\mathfrak{B}_{1/16}(5)$  hold stable organ fates;  $\mathfrak{B}_{1/16}(10)$  and  $\mathfrak{B}_{1/16}(11)$  hold transient inflorescence states.

**Biological Interpretation.** The approximant  $F_4$  correctly classifies all four balls:  $\mathfrak{B}_{1/16}(4)$  and  $\mathfrak{B}_{1/16}(5)$  are 4-contracting and contain the six organ-identity fixed points, while  $\mathfrak{B}_{1/16}(10)$  and  $\mathfrak{B}_{1/16}(11)$  are 4-expanding and contain the four inflorescence fixed points. As a concrete illustration of the ball-level resolution, consider the 512 configurations with prefix (0, 1, 1, 1) in  $\pi^*$  (UFO=0, EMF1=1, LFY=1, TFL1=1, remaining genes arbitrary): they form the ball  $\mathfrak{B}_{1/16}(14)$  (since  $0 \cdot 2^0 + 1 \cdot 2^1 + 1 \cdot 2^2 + 1 \cdot 2^3 = 14$ ) and all converge under  $f$  to the Carpel fixed point (configuration 5492) [18, 27]. The entry  $F_4(\mathfrak{B}_{1/16}(14)) = \mathfrak{B}_{1/128}(0)$  in equation (30) confirms contracting dynamics ( $\Lambda_{4,14} = 1/8$ ). The Carpel fixed point has EMF1=0; the prefix (0, 1, 1, 1) characterizes the *basin*, not the fixed point itself. This confirms that genes in early positions of the  $p$ -adic encoding function as master regulators: their states determine basin membership regardless of downstream gene configurations.

The  $p$ -adic framework identifies key regulatory genes (UFO, LFY, EMF1, TFL1) in leading positions and classifies floral organ identities as either contracting (stable developmental fates) or expanding (transitional states). This classification is consistent with biological understanding: mature floral organs (sepals, petals, stamens, carpels) are stable developmental endpoints, while inflorescence states are transient. Within the Boolean model and its induced dynamics  $f$ , the placement of UFO, LFY, EMF1, and TFL1 as early regulators (via the stability measure  $\mu$ ) agrees with extensive experimental evidence. *LFY* (LEAFY) is a master regulator of floral identity: *lfy* mutants fail to produce flowers and instead develop leaf-like structures [6, 37]; LFY activates floral organ identity genes (AP1, AP3, AG) and is essential for the inflorescence-to-floral meristem transition. *UFO* (UNUSUAL FLORAL ORGANS) specifies

petal and stamen identity; *ufo* mutants exhibit homeotic transformations—petals replaced by sepals, stamens by carpels [10]—consistent with UFO acting as a cofactor whose hierarchical position affects network stability. *EMF1* (EMBRYONIC FLOWER 1) represses flowering and maintains the vegetative state; loss of EMF1 function causes premature flowering [33], supporting its role in developmental timing. *TFL1* (TERMINAL FLOWER 1) maintains inflorescence meristem identity and antagonizes LFY; *tfl1* mutants produce terminal flowers instead of indeterminate inflorescences [32].

That the framework places these four genes in the most significant positions (via minimization of  $\mu$ ) agrees with their established role as master regulators in the literature. The classification of mature floral organs as lying in *contracting* balls (stable fixed points in contracting regions) matches the concept of *canalization* in developmental biology, first proposed by Waddington [36]. Canalization refers to the robustness of developmental processes: once a cell commits to a particular fate (e.g., becoming a petal cell), it maintains that identity despite minor perturbations. This stability is essential for proper organ development and is reflected in our framework as contracting dynamics (ball-level contraction).

Conversely, the classification of inflorescence states as lying in *expanding* balls (expansion at ball level; see Remark 3.17) reflects their transient nature. Inflorescence meristems are developmental intermediates that must progress toward floral organ formation. In the Boolean model, trajectories starting in inflorescence configurations eventually reach floral organ fixed points; biologically, inflorescence meristems persist as indeterminate structures, but the cells they produce commit to specific floral fates. This instability is captured mathematically as expanding dynamics: the image of the ball expands beyond the ball, so that nearby configurations leave the region, consistent with the biological picture of transition toward organ identity.

This interpretation connects our mathematical framework to the classical concept of *epigenetic landscapes* [23], where developmental fates are represented as valleys (attractors) and ridges (repellers) in an energy landscape. A discrete approach to the same GRN, the “Epigenetic Forest” of [29], builds a graph-based representation of Waddington’s landscape from the transition dynamics and recovers flower architecture via optimization of a work function; the present  $p$ -adic framework offers a complementary formulation, replacing energy valleys with ultrametric ball contraction and quantifying hierarchy via the stability measure  $\mu$ .

*Scale-dependent stability classification.* For each fixed point  $a$  with  $f(a) = a$ , the *classification sequence* is the word in  $\{A, E, I\}^{N-1}$  recording the ball classification at each level  $n = 1, \dots, N-1$ ; for instance, IEAA means isometric at  $n=1$ , expanding at  $n=2$ , contracting at  $n=3, 4$ . We propose a scale-dependent classification: for each fixed point, this sequence of ball-level types (contracting, expanding, isometric) across resolution levels. This provides information unavailable from standard Boolean analysis alone. The classification (contracting ‘A’, expanding ‘E’, or isometric ‘I’) at levels  $n = 1, 2, 3, 4$  yields a 4-character sequence per fixed point. This reveals qualitative differences between fixed points that Boolean analysis treats as equivalent.

Config	Ball	Seq.	Type	State	Key genes
436	$B_{1/16}(4)$	IEAA	Contracting	Sepal	LFY, AP1
1972	$B_{1/16}(4)$	IEAA	Contracting	Petal	LFY, AP3
5492	$B_{1/16}(4)$	IEAA	Contracting	Carpel	LFY, AG
6004	$B_{1/16}(4)$	IEAA	Contracting	Stamen	LFY, AG, AP3
1973	$B_{1/16}(5)$	IEAA	Contracting	Petal+UFO	UFO, LFY
6005	$B_{1/16}(5)$	IEAA	Contracting	Stamen+UFO	UFO, LFY, AG
10	$B_{1/16}(10)$	IEEE	Expanding	Inflo.	EMF1, TFL1, LFY=0
2058	$B_{1/16}(10)$	IEEE	Expanding	Inflo.	EMF1, TFL1, WUS
11	$B_{1/16}(11)$	IEEE	Expanding	Inflo.	EMF1, TFL1, UFO
2059	$B_{1/16}(11)$	IEEE	Expanding	Inflo.	EMF1, TFL1, WUS, UFO

Table 4: Classification sequence of fixed points under the ordering  $\pi^*$  (Table 3). Seq. = classification at levels  $n = 1, 2, 3, 4$ ; level  $n = 1$  is I for all balls by (27). Config numbers use the encoding  $m = \sum_{k=0}^{N-1} x_{\alpha_k} 2^k$  with that order. A=contracting, E=expanding, I=isometric; computed from  $\Lambda_{n,m}$ .

(Stamen configurations 6004 and 6005 have AP2=1 in the encoding; this is a property of the Boolean model [18, 27], not an assertion about canonical ABC biology.)

The 10 fixed points partition into two classes by their classification sequences (Table 4). The IEAA pattern (6 fixed points): isometric at level 1, expanding at level 2, then contracting at levels 3–4; these are floral organ identities

(LFY=1), and the system *stabilizes* at fine scales by transitioning from expansion to contraction. The IEEE pattern (4 fixed points): isometric at level 1, then expanding at levels 2–4; these are inflorescence states (TFL1=1, LFY=0), where expansion *persists* across all finer scales. The key distinction is whether the system *stabilizes* (transitions from E to A) at fine scales. Standard Boolean network analysis treats all 10 fixed points as equivalent; the framework distinguishes these two classes and aligns with the observation that inflorescence is a developmental waypoint rather than a terminal state [27]. Part II [30] extends the analysis to *C. elegans* and *D. melanogaster*.

Statistical robustness of the ordering  $\pi^*$  across multiple algorithm runs, and comparison with alternative orderings, is reported in Part II [30]. A detailed analysis of basins of attraction, mutant frequency, and sensitivity to environmental noise is also provided there, where we demonstrate how the basin structure enables quantitative predictions of mutant frequency and robustness to perturbations, with applications to biotechnology.

## 7. Discussion and conclusions

We introduced a hierarchical framework that embeds discrete GRN dynamics into  $\mathbb{Z}_p$  and uses rational approximations  $F_0, \dots, F_N$  to classify ball-level dynamics as  $n$ -contracting,  $n$ -expanding, or  $n$ -isometric at each resolution. The stability measure  $\mu$  is defined from the discrete data  $(f, \iota)$  alone (Theorem 5.5) and satisfies  $\mu_E + \mu_A + \mu_I = (N-1)p^N$  (Lemma 5.2), so that minimizing expansion and maximizing contraction are not equivalent: their optimal orderings can be disjoint (Part II [30]). The  $p$ -adic hierarchy exposes structure that flat attractor analysis cannot: a minimizing ordering places master regulators first, and ball-level contraction separates developmental outcomes—mature organ identities in contracting balls, inflorescence states in expanding ones—in line with canalization [36] and epigenetic landscape models [23, 34]. The ultrametric encodes this quantitatively: configurations agreeing in master-regulator digits are  $p$ -adically close, so downstream variation may converge to one fate while regulator-level differences drive distinct outcomes.

*What the framework adds.* Boolean analysis identifies attractors and basins but treats all configurations in a basin alike. Here,  $\mu$  gives a scalar that quantifies how much expanding behavior appears across scales; in *A. thaliana*,  $\pi^*$  gives  $\mu = 26,776$  while the original-model ordering [18, 27] gives  $\mu = 80,704$  (same  $f$ ). The ball-level classification separates fixed points by local dynamics: under  $\pi^*$ , inflorescence fixed points lie in expanding  $B_{1/16}(10)$  and  $B_{1/16}(11)$ , while organ-identity fixed points lie in contracting  $B_{1/16}(4)$  and  $B_{1/16}(5)$ ; the decomposition  $\mu = \sum_{n=1}^{N-1} |C(n)| p^{N-n}$  shows which levels contribute most (e.g. level  $n = 2$  accounts for about 30.6%). The A/E/I sequence over levels (Table 4) separates fixed points that stabilize at fine scales (IEAA, floral organs) from those that remain expanding (IEEE, inflorescence). All of this is computable from  $(f, \iota)$  alone. Topology-based methods focus on structure; the present framework adds the ultrametric and  $\mu$  so that stability is quantified and orderings compared. Differential-equation models need kinetic parameters; here dynamics remain discrete and the  $p$ -adic side is used for multi-scale classification. Epigenetic landscape approaches [13, 29] also study hierarchical development; the present construction builds hierarchy from  $f$  and an ordering, and  $\mu$  measures how stable that hierarchy is.

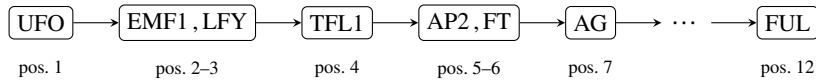
*Hierarchical sensitivity and chaos control.* The coarse multiplier  $\Lambda_{n,m} = p^{n-M_{n,m}}$  is the ball-level analogue of the classical  $p$ -adic multiplier [5, Proposition 3.20]; when  $\Lambda_{n,m} > 1$ , configurations sharing a ball at resolution  $n$  are mapped to a strictly larger ball—loss of predictability at that scale. The measure  $\mu_E$  aggregates these expansion factors across all resolutions, weighted so that coarse-level instability dominates; it may therefore be viewed as a hierarchical, discrete analogue of the Derrida–Pomeau sensitivity parameter for Boolean networks [16], stratified by regulatory depth rather than averaged over the whole network. Minimizing  $\mu_E$  over orderings is, in this reading, a discrete form of chaos control: the optimal hierarchy is the one under which the network dynamics is least sensitive to perturbations at the regulatory level. The evolutionary reading (Section 5) reinforces this: selection favors architectures with low  $\mu_E$  because master-regulator stability is a prerequisite for robust developmental outcomes. Phenotype-control techniques for Boolean networks [31] can build on the hierarchical classification to target resolution-specific interventions.

*Observational interpretation.* Conceptually, the framework separates microscopic states from observable states. A configuration corresponds to a finest-scale ball, whereas larger balls encode coarser observational classes. The dynamics therefore acts not only on individual configurations, but also on families of observables across resolutions. From this viewpoint, contracting, expanding, and isometric behavior describe whether one update decreases, increases,

or preserves observational uncertainty. This reading is natural for biological systems, where exact microstates are rarely measurable and predictions are made at finite resolution.

*Methodological note.* The sole input to the optimization is the transition map  $f : C \rightarrow C$  from the Boolean model [2, 18]; no gene labels, expression data, or prior ranking enter the computation. The measure  $\mu_E$  has no adjustable parameters (equation (24)). That this parameter-free criterion places UFO, EMF1, LFY, and TFL1 in the leading positions—matching the hierarchy established by decades of experimental genetics [6, 27]—is a nontrivial consistency check for a network of  $N=13$  and  $13!$  orderings. Part II [30] tests the framework on three additional networks with distinct topologies.

*Partial order recovered from dynamics.* The formalism explores all  $N!$  total orderings, but the output need not be a single total order. For *A. thaliana*, four orderings attain the same minimal  $\mu_E$ ; their symmetry group  $C_2 \times C_2$  (Remark 6.1) identifies two pairs of interchangeable positions, yielding a *partial order* on genes by hierarchical level:



Genes within a box are interchangeable; arrows indicate strict precedence. The partial order is not imposed but *recovered from the dynamics alone*: EMF1 and LFY (antagonistic in the vegetative-to-floral transition) sit at the same level; AP2 and FT (organ identity vs. flowering timing) are equivalent for  $\mu$ . Developmental hierarchies in the GRN literature are often partially ordered [1, 15]; that minimization of  $\mu$  recovers this structure without presupposing it provides independent mathematical support for the biological picture. Part II [30] examines whether analogous partial-order structure arises in other networks.

*Scope and limitations.* The mathematical framework applies to any finite discrete dynamical system whose state space admits a  $p^N$ -encoding—the sole requirements are a transition map  $f : C \rightarrow C$  and a component ordering. The non-Archimedean analytical structure is not an auxiliary layer but the mathematical engine of the construction: the existence of rational interpreters (Corollary 3.3), the  $\varepsilon$ -approximation technique [28], and  $p$ -adic fixed-point theory [5] are what give the stability measure and the classification their dynamical meaning (Theorem 5.5 and the discussion following it). We use  $p = 2$ ; all definitions and results extend to arbitrary primes. Part II [30] demonstrates this generality on three biologically distinct networks (*C. elegans*, *D. melanogaster*, and a complementary *A. thaliana* analysis); applications to neural, metabolic, and signaling networks are in progress. Minimizing  $\mu$  over  $N!$  orderings is combinatorially hard: for  $N \leq 8$  exhaustive enumeration is feasible; for  $N = 13$ , Part II certifies by branch-and-bound that the ordering reported here is one of four  $\mu_E$ -minimizers, and a genetic algorithm independently recovers it and scales to larger networks. The combinatorial structure of the optimization landscape (submodularity of  $\mu_E$ , computational complexity) remains open; the analogous variable-ordering problem for binary decision diagrams is NP-complete [7]. The framework is Boolean; extension to continuous or stochastic expression levels is future work. The fractal geometry of the  $p$ -adic ball tree suggests natural analogues of Hausdorff-type dimensions for attractor structure and entropic characterizations of the expansion profile; these connections are under investigation and will be developed in a separate work.

In summary, the  $p$ -adic embedding and the measure  $\mu$  yield a quantitative, ordering-dependent view of hierarchical stability that agrees with the known regulatory hierarchy in *A. thaliana* and recovers a partial order on genes from the transition map alone. Part II [30] extends the analysis to *C. elegans* and *D. melanogaster*, develops the comparison between  $\mu_E$ - and  $\mu_A$ -minimizing orderings, and analyzes basin structure and mutant perturbations—confirming that the non-Archimedean framework and the measure  $\mu$  provide a general-purpose tool for the hierarchical analysis of finite discrete dynamical systems.

### Notable orderings for *A. thaliana* ( $N = 13, p = 2$ )

All data in this article are derived from the Boolean model of [18, 27]; the transition map  $f : C \rightarrow C$  is uniquely determined by synchronous update of the regulatory functions. A representative  $\mu_E$ -minimizing ordering  $\pi^*$  with  $\mu(\pi^*) = 26,776$  is reported in the text (Eq. 26, Section 6). Four orderings attain  $\mu_E = 26,776$  (symmetry under transpositions in positions 2–3 and 5–6). Two representative orderings are shown below. Values  $(\mu_E, \mu_A, \mu_I)$ ; the column  $\mu_{AI} = \mu_A + \mu_I$  is included for completeness (the trade-off between  $\mu_E$  and  $\mu_A$  is analyzed in Part II [30]).

Label	Ordering (genes)	$\mu_E$	$(\mu_A, \mu_I)$	$\mu_{AI}$
$\pi^*$ (paper)	UFO, EMF1, LFY, TFL1, AP2, FT, AG, AP1, SEP, AP3, PI, WUS, FUL	26,776	(53,880, 17,648)	71,528
Alternative	UFO, LFY, EMF1, TFL1, FT, AP2, AG, AP1, SEP, AP3, PI, WUS, FUL	26,776	(53,880, 17,648)	71,528

The four orderings share the same tail (positions 7–13) and the same  $(\mu_E, \mu_A, \mu_I)$ ; the two rows above are representatives.

## Declarations

### Funding

This work was supported by the project “Modelos matemáticos y computacionales no convencionales para el estudio y análisis de problemas relevantes en Biología” (CF 2019/217367) funded by SECIHTI, and by the Proyecto de Frontera.

### Competing interests

The authors declare that they have no competing interests.

### Authors' contributions

J.R.-P.B. and V.-N.C. conceived and developed the mathematical framework and the theoretical content of this paper, and wrote the manuscript. Both authors read and approved the final manuscript.

### Data availability

The transition map  $f$  is determined by the Boolean model in the cited references. The full transition table and the reported orderings (see the table above) can be provided by the corresponding author upon reasonable request.

### Acknowledgments

We thank the P-adagio working group and the p-adic research group for their support, and Esteban Sánchez Durán for his contributions in the early stages of this project, including the creation of the first models and computational implementations during his period as a research fellow in the Proyecto de Frontera “Modelos matemáticos y computacionales no convencionales para el estudio y análisis de problemas relevantes en Biología” (CF 2019/217367) funded by SECIHTI. This collaboration was developed during V. Nopal-Coello's postdoctoral appointment at CIMAT Mérida under the mentorship of J. R. Pérez-Buendía.

## References

- [1] Alon, U., 2006. An Introduction to Systems Biology: Design Principles of Biological Circuits. Chapman and Hall/CRC, Boca Raton, FL. URL: <https://doi.org/10.1201/9781420011432>, doi:doi:10.1201/9781420011432.
- [2] Alvarez-Buylla, E.R., Benítez, M., Balleza Dávila, E., Chaos, A., Espinosa-Soto, C., Padilla-Longoria, P., 2007. Gene regulatory network models for plant development. *Current Opinion in Plant Biology* 10, 83–91. URL: <https://doi.org/10.1016/j.pbi.2006.11.008>, doi:doi:10.1016/j.pbi.2006.11.008.
- [3] Ashcroft, N., Golden, A., 2002. Cdc-25.1 regulates germline proliferation in caenorhabditis elegans. *Genesis* 33, 1–7. URL: <https://doi.org/10.1002/gene.10083>, doi:doi:10.1002/gene.10083.
- [4] Barabási, A.L., Oltvai, Z.N., 2004. Network biology: Understanding the cell's functional organization. *Nature Reviews Genetics* 5, 101–113. URL: <https://doi.org/10.1038/nrg1272>, doi:doi:10.1038/nrg1272.
- [5] Benedetto, R.L., 2019. Dynamics in one non-archimedean variable. volume 198 of *Graduate Studies in Mathematics*. American Mathematical Soc. URL: <https://doi.org/10.1090/gsm/198>, doi:doi:10.1090/gsm/198.
- [6] Blázquez, M.A., Soowal, L.N., Lee, I., Weigel, D., 1997. Leafy expression and flower initiation in arabidopsis. *Development* 124, 3835–3844. URL: <https://doi.org/10.1242/dev.124.19.3835>, doi:doi:10.1242/dev.124.19.3835.
- [7] Bollig, B., Wegener, I., 1996. Improving the variable ordering of OBDDs is NP-complete, in: STACS 96, Springer. pp. 81–92. doi:doi:10.1007/3-540-60922-9\_7.
- [8] Bornholdt, S., 2005. Systems biology: Less is more in modeling large genetic networks. *Science* 310, 449–451. URL: <https://doi.org/10.1126/science.1119959>, doi:doi:10.1126/science.1119959.
- [9] Boxem, M., 2006. Cyclin-dependent kinases in c. elegans. *Cell Division* 1, 6. URL: <https://doi.org/10.1186/1747-1028-1-6>, doi:doi:10.1186/1747-1028-1-6.
- [10] Chae, E., Tan, Q.K.C., Hill, T.A., Irish, V.F., 2008. An arabidopsis f-box protein acts as a transcriptional co-factor to regulate floral development. *Development* 135, 1235–1245. URL: <https://doi.org/10.1242/dev.015842>, doi:doi:10.1242/dev.015842.
- [11] Chaves, M., Albert, R., Sontag, E.D., 2005. Robustness and fragility of boolean models for genetic regulatory networks. *Journal of Theoretical Biology* 235, 431–449. URL: <https://doi.org/10.1016/j.jtbi.2005.01.023>, doi:doi:10.1016/j.jtbi.2005.01.023.

- [12] Chávez-Hernández, E.C., Quiroz, S., García-Ponce, B., Álvarez-Buylla, E.R., 2022. The flowering transition pathways converge into a complex gene regulatory network that underlies the phase changes of the shoot apical meristem in *Arabidopsis thaliana*. *Frontiers in Plant Science* 13, 852047. doi:doi:10.3389/fpls.2022.852047.
- [13] Cortés-Poza, Y., Padilla-Longoria, P., 2022. A variational approach to morphogenesis: Recovering spatial phenotypic features from epigenetic landscapes. *Bulletin of Mathematical Biology* 84, 33. URL: <https://doi.org/10.1007/s11538-022-00993-w>, doi:doi:10.1007/s11538-022-00993-w.
- [14] Davidich, M.I., Bornholdt, S., 2008. Boolean network model predicts cell cycle sequence of fission yeast. *PLoS ONE* 3, e1672. URL: <https://doi.org/10.1371/journal.pone.0001672>, doi:doi:10.1371/journal.pone.0001672.
- [15] Davidson, E.H., Erwin, D.H., 2006. Gene regulatory networks and the evolution of animal body plans. *Science* 311, 796–800. URL: <https://doi.org/10.1126/science.1113832>, doi:doi:10.1126/science.1113832.
- [16] Derrida, B., Pomeau, Y., 1986. Random networks of automata: a simple annealed approximation. *Europhysics Letters* 1, 45–49. doi:doi:10.1209/0295-5075/1/2/001.
- [17] Dragovich, B., Khrennikov, A.Y., Kozyrev, S.V., Mišić, N.Ž., 2021.  $p$ -adic mathematics and theoretical biology. *Biosystems* 199, 104288. URL: <https://doi.org/10.1016/j.biosystems.2020.104288>, doi:doi:10.1016/j.biosystems.2020.104288.
- [18] Espinosa-Soto, C., Padilla-Longoria, P., Álvarez-Buylla, E.R., 2004. A gene regulatory network model for cell-fate determination during *Arabidopsis thaliana* flower development that is robust and recovers experimental gene expression profiles. *The Plant Cell* 16, 2923–2939. URL: <https://doi.org/10.1105/tpc.104.021725>, doi:doi:10.1105/tpc.104.021725.
- [19] Fuquen-Tibatá, A., Cortés-Poza, Y., Pérez-Buendía, J.R., 2026. A  $p$ -adic reaction–diffusion model of branching coral growth and calcification dynamics. *Journal of Mathematical Biology* 92, 27. URL: <https://doi.org/10.1007/s00285-025-02340-8>, doi:doi:10.1007/s00285-025-02340-8.
- [20] Glass, L., Kauffman, S.A., 1973. The logical analysis of continuous, non-linear biochemical control networks. *Journal of Theoretical Biology* 39, 103–129. URL: [https://doi.org/10.1016/0022-5193\(73\)90208-7](https://doi.org/10.1016/0022-5193(73)90208-7), doi:doi:10.1016/0022-5193(73)90208-7.
- [21] Gouvêa, F.Q., 2020.  $p$ -adic Numbers: An Introduction. Universitext. 3rd ed., Springer, Cham. doi:doi:10.1007/978-3-030-47295-5.
- [22] Haury, A.C., Mordelet, F., Vera-Licona, P., Vert, J.P., 2012. Tigress: Trustful inference of gene regulation using stability selection. *BMC Systems Biology* 6, 145. URL: <https://doi.org/10.1186/1752-0509-6-145>, doi:doi:10.1186/1752-0509-6-145.
- [23] Huang, S., 2012. The molecular and mathematical basis of waddington’s epigenetic landscape: A framework for post-darwinian biology? *BioEssays* 34, 149–157. URL: <https://doi.org/10.1002/bies.201100031>, doi:doi:10.1002/bies.201100031.
- [24] Kadelka, C., Butrie, T.M., Hilton, E., Kinseth, J., Schmidt, A., Serdarevic, H., 2024. A meta-analysis of Boolean network models reveals design principles of gene regulatory networks. *Science Advances* 10, eadj0822. doi:doi:10.1126/sciadv.adj0822.
- [25] Kauffman, S.A., 1969. Metabolic stability and epigenesis in randomly constructed genetic nets. *Journal of Theoretical Biology* 22, 437–467. URL: [https://doi.org/10.1016/0022-5193\(69\)90015-0](https://doi.org/10.1016/0022-5193(69)90015-0), doi:doi:10.1016/0022-5193(69)90015-0.
- [26] Li, F., Long, T., Lu, Y., Ouyang, Q., Tang, C., 2004. The yeast cell-cycle network is robustly designed. *Proceedings of the National Academy of Sciences* 101, 4781–4786. URL: <https://doi.org/10.1073/pnas.0305937101>, doi:doi:10.1073/pnas.0305937101.
- [27] Mendoza, L., Álvarez-Buylla, E.R., 1998. Dynamics of the genetic regulatory network for *Arabidopsis thaliana* flower morphogenesis. *Journal of Theoretical Biology* 193, 307–319. URL: <https://doi.org/10.1006/jtbi.1998.0701>, doi:doi:10.1006/jtbi.1998.0701.
- [28] Nopal Coello, V., Pérez-Buendía, J.R., 2025. Gluing dynamics:  $\epsilon$ -precision in solving a non-archimedean inverse problem. *Boletín de la Sociedad Matemática Mexicana* 31, 52. URL: <https://doi.org/10.1007/s40590-025-00730-y>, doi:doi:10.1007/s40590-025-00730-y.
- [29] Pérez-Buendía, J.R., Cortés-Poza, Y., Padilla-Longoria, P., 2022. Epigenetic forest and flower morphogenesis. *Computational Biology and Chemistry* 98, 107667. URL: <https://doi.org/10.1016/j.compbiolchem.2022.107667>, doi:doi:10.1016/j.compbiolchem.2022.107667.
- [30] Pérez-Buendía, J.R., Nopal-Coello, V., Cortés-Poza, Y., 2026. Hierarchical  $p$ -adic framework for gene regulatory networks: Part II—Applications and comparative analysis. In preparation.
- [31] Plaughter, D., Murrugarra, D., 2023. Phenotype control techniques for Boolean gene regulatory networks. *Bulletin of Mathematical Biology* 85, 89. doi:doi:10.1007/s11538-023-01197-6.
- [32] Shannon, S., Meeks-Wagner, D.R., 1991. A mutation in the *Arabidopsis thaliana* *ft1* gene affects inflorescence meristem development. *The Plant Cell* 3, 877–892. URL: <https://doi.org/10.1105/tpc.3.9.877>, doi:doi:10.1105/tpc.3.9.877.
- [33] Sung, Z.R., Belachew, A., Shunong, B., Bertrand-Garcia, R., 1992. *Emf*, an *Arabidopsis* gene required for vegetative shoot development. *Science* 258, 1645–1647. URL: <https://doi.org/10.1126/science.258.5090.1645>, doi:doi:10.1126/science.258.5090.1645.
- [34] Trinh, V.G., Park, K.H., Pastva, S., Rozum, J.C., 2025. Mapping the attractor landscape of Boolean networks with biobalm. *Bioinformatics* 41, btaf280. doi:doi:10.1093/bioinformatics/btaf280.
- [35] Vera-Licona, P., Jarrah, A., García-Puente, L.D., McGee, J., Laubenbacher, R., 2014. An algebra-based method for inferring gene regulatory networks. *BMC Systems Biology* 8, 37. URL: <https://doi.org/10.1186/1752-0509-8-37>, doi:doi:10.1186/1752-0509-8-37.
- [36] Waddington, C.H., 1957. *The Strategy of the Genes*. Allen & Unwin, London, UK. URL: <https://www.routledge.com/The-Strategy-of-the-Genes/Waddington/p/book/9781138998131>. classic work on developmental biology and epigenetics. Reprint: Routledge, 2015, ISBN 9781138998131.
- [37] Weigel, D., Alvarez, J., Smyth, D.R., Yanofsky, M.F., Meyerowitz, E.M., 1992. Leafy controls floral meristem identity in *Arabidopsis*. *Cell* 69, 843–859. URL: [https://doi.org/10.1016/0092-8674\(92\)90295-N](https://doi.org/10.1016/0092-8674(92)90295-N), doi:doi:10.1016/0092-8674(92)90295-N.
- [38] Zambrano-Luna, B.A., Zúñiga-Galindo, W.A., 2023.  $p$ -adic cellular neural networks. *Journal of Nonlinear Mathematical Physics* 30, 34–70. doi:doi:10.1007/s44198-022-00071-8.
- [39] Zúñiga-Galindo, W.A., 2018. Non-archimedean replicator dynamics and eigen’s paradox. *Journal of Physics A: Mathematical and Theoretical* 51, 505601. URL: <https://doi.org/10.1088/1751-8121/aaebb1>, doi:doi:10.1088/1751-8121/aaebb1.
- [40] Zúñiga-Galindo, W.A., 2021. Non-Archimedean models of morphogenesis, in: Zúñiga-Galindo, W.A., Toni, B. (Eds.), *Advances in Non-Archimedean Analysis and Applications*. Springer, Cham. STEAM-H, pp. 255–274. doi:doi:10.1007/978-3-030-81976-7\_7.

- [41] Zúñiga-Galindo, W.A., 2022.  $p$ -adic analysis: A quick introduction, in: Galindo, C., Melle Hernández, A., Moyano-Fernández, J., Zúñiga-Galindo, W. (Eds.),  $p$ -Adic Analysis, Arithmetic and Singularities. American Mathematical Society, Providence, RI. volume 778 of *Contemporary Mathematics*, pp. 253–292. URL: <https://doi.org/10.1090/conm/778>, doi:doi:10.1090/conm/778. mini-Course, L. Santaló Research Summer School 2019, Santander, Spain.
- [42] Zúñiga-Galindo, W.A., 2025.  $p$ -Adic Analysis: Stochastic Processes and Pseudo-Differential Equations. volume 11 of *Advances in Analysis and Geometry*. De Gruyter, Berlin. doi:doi:10.1515/9783111578682.